

Supervised-Contrastive Loss Learns Orthogonal Frames and Batching Matters

Ganesh Ramachandra Kini[‡], Vala Vakilian[†], Tina Behnia[†], Jaidev Gill[†], Christos Thrampoulidis[†]

[‡]University of California, Santa Barbara, USA

[†]University of British Columbia, Canada ^{*}

June 14, 2023

Abstract

Supervised contrastive loss (SCL) is a competitive and often superior alternative to the cross-entropy (CE) loss for classification. In this paper we ask: what differences in the learning process occur when the two different loss functions are being optimized? To answer this question, our main finding is that the geometry of embeddings learned by SCL forms an orthogonal frame (OF) regardless of the number of training examples per class. This is in contrast to the CE loss, for which previous work has shown that it learns embeddings geometries that are highly dependent on the class sizes. We arrive at our finding theoretically, by proving that the global minimizers of an unconstrained features model with SCL loss and entry-wise non-negativity constraints form an OF. We then validate the model’s prediction by conducting experiments with standard deep-learning models on benchmark vision datasets. Finally, our analysis and experiments reveal that the batching scheme chosen during SCL training plays a critical role in determining the quality of convergence to the OF geometry. This finding motivates a simple algorithm wherein the addition of a few *binding examples* in each batch significantly speeds up the occurrence of the OF geometry.

Code available [here](#).

1 Introduction

The prevalence of deep-neural networks (DNNs) has led to a growing research interest in understanding their underlying mechanisms. A recent research thread, focusing on classification tasks, explores whether it is possible to describe the structure of weights learned by DNNs when trained beyond zero-training error. The specific characteristics of this structure will depend on the DNN being used, the dataset being trained on, and the chosen optimization hyperparameters. However, *can we identify macroscopic structural characteristics that are common among these possibilities?*

In an inspiring study, [PHD20] demonstrates this is possible for the classifiers and for the embeddings when training with cross-entropy (CE) loss. Through extensive experiments over multiple architectures and balanced datasets with an equal number of examples per class, they found that the geometries of classifiers and of centered class-mean embeddings (i.e., outputs of the last hidden layer) consistently converge during training to a common simplex equiangular tight frame (ETF), a structure composed of vectors that have equal norms and equal angles between them, with the angles being the maximum possible. Moreover, neural-collapse (NC), a

^{*}This work is supported by an NSERC Discovery Grant, NSF Grant CCF-2009030, and by a CRG8-KAUST award. JG and CT gratefully acknowledge the support of NSERC Undergraduate Student Research Grant. The authors also acknowledge use of the Sockeye cluster by UBC Advanced Research Computing.

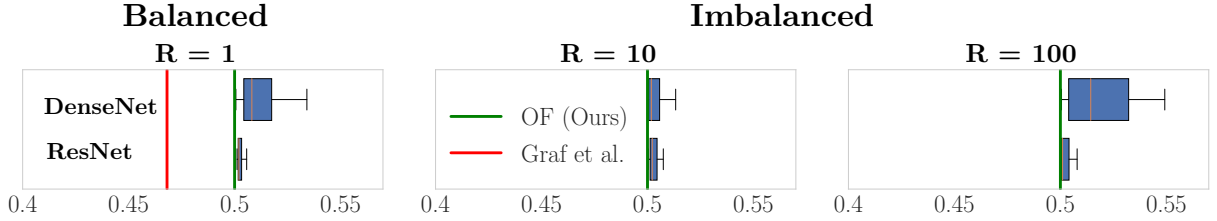


Figure 1: Experimental validation of our key finding: SCL learns orthogonal class-mean embeddings irrespective of class imbalances. Shown are box plots of pairwise angular distance $\Delta_{\text{ang}} = 1 - 1/\pi \arccos(\mu_c^\top \mu_{c'}/\|\mu_{c'}\| \|\mu_c\|)$ between class-mean embeddings $\mu_c, \mu_{c'}, c \neq c' \in [k]$ of a ResNet-18 (bottom) and DenseNet-40 (top) trained with SCL on R -STEP-imbalanced CIFAR-10. In all three cases, our prediction highlighted in green and corresponding to an orthogonal angle is remarkably close to the measurements. Compare to the red line predicted by [Gra+21] for balanced data. No explicit characterization has been known previously for imbalanced data.

property where embeddings of individual examples from each class converge to their class-mean embedding, was also observed. Numerous follow-up studies have delved deeper into explaining this phenomenon and further investigating how the converging geometry changes with class imbalances. The unconstrained-features model (UFM), proposed by [MPP20; Fan+21; Gra+21; Ji+21; LS20; TB22], plays a central role in the majority of these follow-up studies. Specifically, the UFM serves as a theoretical abstraction for DNN training, in which the network architecture is viewed as a powerful black-box that generates embeddings without any restrictions in the last (hidden) layer. For CE loss, the UFM minimizes $\min_{\mathbf{w}_c \in \mathbb{R}^d, \mathbf{h}_i \in \mathbb{R}^d} \mathcal{L}_{\text{CE}}(\{\mathbf{w}_c\}_{c \in [k]}, \{\mathbf{h}_i\}_{i \in [n]})$ in which both classifiers \mathbf{w}_c for the k classes and embeddings \mathbf{h}_i for the n training examples are unconstrainedly optimized over \mathbb{R}^d . [Zhu+21; Gra+21; Fan+21] have verified that the global minimum of this non-convex problem satisfies NC and follows the ETF geometry observed in DNN experiments by [PHD20]. Interestingly, recent works by [Thr+22; Fan+21; Beh+23] have demonstrated that the global optimum of the UFM changes when classes are imbalanced. However, the new solution still predicts the geometry observed in DNN experiments, providing evidence that, despite its oversimplification, the UFM is valuable in predicting structural behaviors.

Expanding beyond the scope of CE minimization, [Gra+21] also used the UFM to determine whether optimizing with the supervised-contrastive loss (SCL) results in any alterations to the geometric structure of the learned embeddings.¹ They proved for balanced datasets that the global solution of $\min_{\mathbf{h}_i \in \mathbb{R}^d} \mathcal{L}_{\text{SCL}}(\{\mathbf{h}_i\}_{i \in [n]})$ remains a simplex ETF. This suggested that CE and SCL find the same embedding geometries. In order to verify this empirically, they trained a ResNet-18 on CIFAR10 and calculated the angular distance between the class-mean embeddings $\mu_c, \mu_{c'}$ for $c \neq c'$. In Fig. 1(a), we have reproduced their experiment and presented a boxplot illustrating the distribution of the measured angular distances. Note that the angular distance value, as predicted by the analysis carried out in [Gra+21] and highlighted in red, shows a slight deviation from the measured values. Moreover, their prediction only applies to balanced data and no prior work has explicitly characterized the geometry of SCL loss *with* class imbalances. These observations give rise to the following research questions motivating our work:

When classes are balanced, what could account for the difference between the UFM prediction from [Gra+21] and the experimental values in Fig. 1(a)? Is the UFM unable to accurately predict the geometry learned by SCL? Additionally, what is the geometry of the embeddings under imbalances? Ultimately, is the implicit geometry of embeddings the same when optimizing with either the CE or the SCL loss?

¹SCL is designed to train only embeddings and is an extension of the well-known contrastive loss used for unsupervised learning, adapted to supervised datasets [Kho+20]; see Equation (2).

1.1 Summary of contributions

This paper answers all the above questions.

Key finding. We find that SCL learns class-mean embeddings that are pairwise orthogonal, hence they form an orthogonal frame (OF), a structure composed of vectors that have equal norms and are mutually orthogonal to each other. Interestingly, this geometry remains consistent regardless of the label distribution, i.e., the number of examples per class. This finding highlights a notable distinction between SCL and CE loss, as the geometry of embeddings learnt with CE is known to be highly-influenced by the label distribution.

Experimental justification. An initial experimental validation of our finding is illustrated in Fig. 1. The experiments correspond to STEP-imbalanced CIFAR-10 data with five majority/minority classes and imbalance ratio $R = 1, 10, 100$. The green line highlights the angular distance of orthogonal angles (corresponding to an OF), which is $1/2$, and remarkably aligns with the measured angles for *all* values of the imbalance ratio R . Extensive additional experiments for Long-tailed (LT) distributions, other datasets, and architectures, are presented in Sec. 3 and Sec. D in the appendix.

Theoretical justification. Our finding emerged through theoretical analysis by investigating the global minimizers of an extended version, denoted as UFM_+ , of the original unconstrained-features model (UFM). This refinement accounts for the presence of ReLU activations in the last hidden layer of commonly used architectures by minimizing the SCL over the non-negative orthant. Concretely, we show that all global solutions of $\min_{\mathbf{h}_i \geq 0} \mathcal{L}_{\text{SCL}}(\{\mathbf{h}_i\}_{i \in [n]})$ satisfy NC and the corresponding class-mean features form an OF. This explains the implicit geometry observed in our experiments, eliminating the requirement for a heuristic centering of the class-mean embeddings as implemented in the majority of prior studies.

Analysis of batching and implications. Finally, we examine the impact of batching on determining the learned embedding geometry. By utilizing the UFM_+ , we establish straightforward criteria for the batching scheme, ensuring that any global minimizer forms an OF. By utilizing these conditions, we provide an explanation for the observed substantial degradation in convergence towards an OF when employing a fixed batch partition instead of randomly reshuffling the batches at each training epoch. Intriguingly, we demonstrate that any arbitrary batching partition can be transformed into one that fulfills our theoretical conditions by introducing k so-called “binding examples” in each batch. Moreover, as verified in Sec. 5.2, this approach consistently accelerates the convergence of the learned geometry towards an OF.

1.2 Organization

The remaining portion of the paper is organized as follows. In Sec. 2, we formally introduce the SCL and provide an overview of the OF geometry. Sec. 3 presents and discusses the experimental evidence that supports our main finding. The theoretical justification for our finding is presented in Sec. 4, where we analyze both full-batch and mini-batch SCL scenarios. Building upon the insights gained from the analysis of mini-batch SCL, Sec. 5 explores the critical role of batching and proposes a binding-examples scheme aimed at enhancing the convergence quality of the implicit geometry. To position our results in the context of related works, Sec. 6 further discusses the most closely related studies and presents a detailed comparison between the UFM_+ model, which we rely on in this paper, and the previously-used UFM. Sec. 7 concludes the paper by reflecting on the contribution of our findings and discussing their implications at the intersection of the literature on neural-collapse phenomena and contrastive-type losses. The appendix contains all the proofs, along with additional experimental details and supplementary experiments.

Notation. For a positive integer n , we denote $[n] := \{1, 2, 3, \dots, n\}$. For matrix $\mathbf{V} \in \mathbb{R}^{m \times n}$,

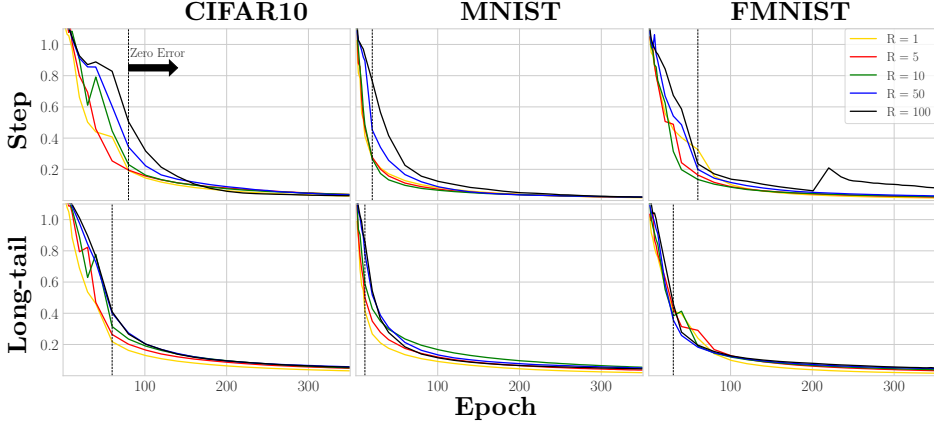


Figure 2: ResNet-18 model trained on imbalanced datasets with SCL. Convergence of last-layer embeddings to the OF geometry as measured by $\Delta_{\mathbf{G}_M} := \left\| \frac{\mathbf{G}_M}{\|\mathbf{G}_M\|_F} - \frac{\mathbb{I}_k}{\|\mathbb{I}_k\|_F} \right\|_F$, where $\mathbf{G}_M = \mathbf{M}^\top \mathbf{M}$ is the Gram matrix of class-mean embeddings. $\Delta_{\mathbf{G}_M}$ is consistently on the order of 0.01 regardless of dataset or imbalance.

$\mathbf{V}[i, j]$ denotes its (i, j) -th entry, \mathbf{v}_j denotes the j -th column, \mathbf{V}^\top its transpose. We denote $\|\mathbf{V}\|_F$ the Frobenius norm of \mathbf{V} . We use $\mathbf{V} \propto \mathbf{X}$ whenever the two matrices are equal up to a scalar constant. We use $\mathbf{V} \geq 0$ to denote the entry-wise non-negativity of the elements of \mathbf{V} , i.e., $\mathbf{V}[i, j] \geq 0, \forall i \in [m], j \in [n]$. Finally, \mathbb{I}_m denotes the identity matrix of size m .

2 Setup

Consider k -class classification and training set $S = \{(\mathbf{x}_i, y_i) : i \in [n]\}$ where $\mathbf{x}_i \in \mathbb{R}^d$, $y_i \in [k]$ represent data samples and corresponding class labels. We use n_c to denote the number of examples in class $c \in [k]$, and $\mathbf{h}_\theta(\cdot)$ to denote the last-layer feature-embeddings of a deep-net parameterized by θ . We compute the SCL on a given batch $B \subseteq [n]$ of training examples as follows,

$$\mathcal{L}_B(\theta) := \sum_{i \in B} \frac{1}{n_{B, y_i} - 1} \sum_{\substack{j \in B \\ y_j = y_i, j \neq i}} \log \left(1 + \sum_{\ell \neq i, j} \exp \left(\frac{1}{\tau} (\mathbf{h}_\theta(\mathbf{x}_i)^\top \mathbf{h}_\theta(\mathbf{x}_\ell) - \mathbf{h}_\theta(\mathbf{x}_i)^\top \mathbf{h}_\theta(\mathbf{x}_j)) \right) \right), \quad (1)$$

where τ is a positive scalar temperature hyper-parameter, and n_{B, y_i} is the number of examples in batch B belonging to class $c = y_i$. To train a deep-net, we minimize SCL (1) over the network parameters θ on a set of batches \mathcal{B} chosen from the training set. As introduced by Khosla et al. [Kho+20], SCL requires normalized features, so we assume $\|\mathbf{h}_\theta(\mathbf{x}_i)\| = 1$. Furthermore, throughout this paper, we assume that $d \geq k$ and $n_c, n_{B, c} \geq 2, c \in [k]$.²

We let $\mathbf{H}_{d \times n} = [\mathbf{h}_1, \dots, \mathbf{h}_n]$ denote an embeddings matrix where each column corresponds to one of the examples in the training set, i.e., $\mathbf{h}_i := \mathbf{h}_\theta(\mathbf{x}_i)$. The *embeddings geometry* or so-called *implicit geometry*³ refers to the norms and pairwise-angles of these vectors $\mathbf{h}_i, i \in [n]$. Note these quantities correspond exactly to the entries of the Gram matrix $\mathbf{H}^\top \mathbf{H}$. In order to characterize the geometry, we need the following definitions.

Definition 1 (Neural Collapse (NC)). *NC occurs if $\mathbf{h}_i = \mathbf{h}_j, \forall i, j : y_i = y_j$.*

²When using SCL, it is common practice to add an augmented version of the datapoints in each batch to itself [Kho+20; Gra+21]. This practice, referred to as *batch duplication* [Gra+21], helps ensure that each datapoint in a batch has at least one other example in the same class to compare to during training.

³The specific terminology is adopted from [Beh+23].

Definition 2 (*k*-Orthogonal Frame (*k*-OF)). *We say that k vectors $\mathbf{V} = [\mathbf{v}_1, \dots, \mathbf{v}_k] \in \mathbb{R}^{d \times k}$ form a *k*-OF if $\mathbf{V}^\top \mathbf{V} \propto \mathbb{I}_k$, i.e., for each pair of $(i, j) \in [k]$, $\|\mathbf{v}_i\| = \|\mathbf{v}_j\|$ and $\mathbf{v}_i^\top \mathbf{v}_j = 0$.*

When the within-class variation of embeddings is negligible, i.e., \mathbf{H} satisfies NC, it suffices to focus on the class-mean embeddings $\boldsymbol{\mu}_c = \frac{1}{n_c} \sum_{i:y_i=c} \mathbf{h}_i$, $c \in [k]$ and their respective matrix $\mathbf{M}_{d \times k} = [\boldsymbol{\mu}_1, \dots, \boldsymbol{\mu}_k]$. That is, it suffices to study $\mathbf{G}_M = \mathbf{M}^\top \mathbf{M}$ instead of $\mathbf{H}^\top \mathbf{H}$. With these, we can formally define the OF geometry for embeddings \mathbf{H} as follows.

Definition 3 (OF geometry). *We say that a feature-embedding matrix \mathbf{H} follows an OF geometry if it satisfies NC and the class-means form a *k*-OF, i.e., $\mathbf{G}_M \propto \mathbb{I}_k$.*

3 SCL learns OF geometries: Empirical findings

Experimental setup. We study the behavior of models trained with SCL under, 1) *R-STEP* imbalance having $k/2$ majority classes with n_{maj} datapoints per class and $k/2$ minority classes with $n_{\text{min}} = \frac{n_{\text{maj}}}{R}$ datapoints per class, and 2) *R-Long-tailed* (LT) imbalance where the number of training datapoints exponentially decreases across classes such that $n_c = n_1 R^{-(c-1/k-1)}$, for $c \in [k]$. Regardless of the imbalance ratio R , we ensure that $n_c \geq 2$ by adding a vertically flipped version of each image as a method of batch duplication. Unless explicitly stated, we do not perform any additional data augmentation on the datasets, and use a batch size of 1024 with random reshuffling. We minimize SCL using Stochastic Gradient Descent (SGD) with a constant learning rate of 0.1, and momentum set to 0.9 with no weight decay. Furthermore, as in [Gra+21; Kho+20], we set the temperature parameter $\tau = 0.1$. We empirically find that convergence to OF is not highly dependent on τ for values near 0.1, yet the specific choice affects the speed of convergence. Besides this, Khosla et al. [Kho+20] have found that $\tau = 0.1$ leads to the best generalization performance. In all cases, network architectures (ResNet-18 etc.) normalize features to unit norm before the output as discussed in [Kho+20]. Link to the codebase to reproduce experiments is provided [here](#).

Metrics. Since in all experiments we observe the within-class variations of the last-layer embeddings (\mathbf{h}_i) become negligible towards the end of training (see NC plots in Fig. 10 in the appendix), we focus here on the geometry of class-mean embeddings \mathbf{M} . Thus, to measure the distance of learned embedding to the OF geometry, we compute the distance metric $\Delta_{\mathbf{G}_M} := \|\frac{\mathbf{G}_M}{\|\mathbf{G}_M\|_F} - \frac{\mathbb{I}_k}{\|\mathbb{I}_k\|_F}\|_F$. In addition, we measure the pairwise cosine similarity $\alpha_{\text{sim}}(c, c') := \boldsymbol{\mu}_c^\top \boldsymbol{\mu}_{c'} / \|\boldsymbol{\mu}_c\| \|\boldsymbol{\mu}_{c'}\|$ for $c \neq c' \in [k]$. Finally, for ease of comparison with results of Graf et al. [Gra+21], we also compute the corresponding angular distance $\Delta_{\text{ang}} := 1 - 1/\pi \arccos(\alpha_{\text{sim}}(c, c'))$.

Observations. In Fig. 2, we plot the distance $\Delta_{\mathbf{G}_M}$ between the learned feature-embeddings and the OF geometry as training progresses. Across our deep-net experiments, we consistently observe that the learned features during training converge to the OF geometry, irrespective of the imbalance level R of the training set and the imbalance pattern (STEP or LT). This suggests that the feature geometry learned by SCL is invariant to the training label distribution.

This property contrasts with that of CE and MSE loss which are known to be sensitive to imbalances [Thr+22; Fan+21; Liu+23; Beh+23; Dan+23]. Additionally, for different values of R , there is no significant difference between the speed of convergence, unlike the CE loss [Thr+22], where it is empirically observed that the rate worsens with larger imbalance levels.

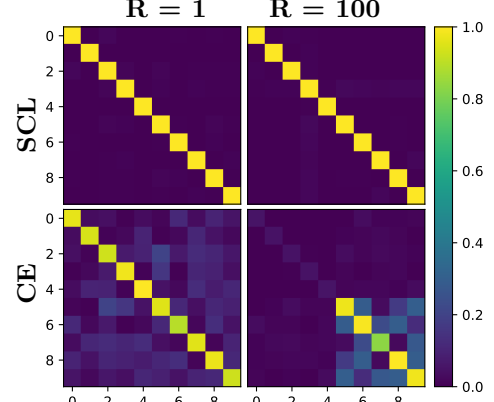


Figure 3: \mathbf{G}_M at last epoch (350) for ResNet-18 trained on *R*-STEP imbalanced MNIST. See text for details.

Lastly, Fig. 3 compares the heatmap of \mathbf{G}_M at last epoch 350 learned by SCL and CE losses over R -STEP imbalanced MNIST. For better comparison, in each experiment, we normalize \mathbf{G}_M by the maximum entry (i.e., we normalize the class-mean features to have a maximum norm of 1). We observe that in case of CE with high imbalance ratio R , the class-mean embeddings representing different minority classes are closer to each other (have smaller angles) compared to that of SCL; see Fig. 3, $R = 100$.

Remark 1. *Contrary to previous claims in the literature, our findings challenge the notion that the embeddings geometry of SCL becomes asymmetric under imbalances, as suggested by Zhu et al. [Zhu+22]. Instead, our results indicate that the geometry remains an OF, regardless of the presence of class imbalance. It is important to highlight that the primary focus and main contribution of [Zhu+22] revolve around their proposed variant of SCL, called the balanced contrastive loss (BCL), which they empirically demonstrate achieves state-of-the-art performance in long-tailed image classification tasks. Nevertheless, our findings raise an intriguing research question that challenges the justification for BCL given in [Zhu+22], particularly the claim that it enforces symmetric geometric structures unlike SCL. In particular, this prompts further investigation into understanding the underlying factors that make BCL more resilient to distributional variations compared to SCL.*

4 Theoretical justification: SCL with non-negativity constraints

In this section, we analytically justify the convergence of the embeddings learned by SCL to the OF geometry. For our theoretical analysis, we use the Unconstrained Features Model (UFM) [MPP20; Fan+21; Gra+21; Ji+21; LS20; TB22], where we treat the last-layer features \mathbf{H} as free variables, removing the dependence to the network parameters θ . However, we refine the UFM, and consider the SCL minimization over the non-negative orthant to accommodate for the presence of ReLU activations in the last layer of many common architectures.⁴ We further constrain the embeddings \mathbf{h}_i to be normalized as we saw this is inherent in the SCL optimization [Kho+20]. We prove, irrespective of the labels distribution, that the global optimizers form an OF. Formally, consider the following refined UFM for SCL, which we call UFM_+ for convenience:

$$\widehat{\mathbf{H}} \in \arg \min_{\mathbf{H}} \mathcal{L}_{\text{SCL}}(\mathbf{H}) \text{ subj. to } \mathbf{H} \geq 0 \text{ and } \|\mathbf{h}_i\|^2 = 1, \forall i \in [n]. \quad (\text{UFM}_+)$$

Recall $\mathbf{H} \geq 0$ denotes entry-wise non-negativity. We begin our analysis by considering the full-batch version of the loss in Sec. 4.1, and subsequently extend our results to the SCL minimized on mini-batches as in (1) in Sec. 4.2. We provide specific conditions that mini-batches must satisfy in order to have the same global optimum as the full-batch version.

4.1 Full-batch SCL

Here, we focus on the full-batch SCL, where the entire training set is treated as a single batch. Specifically, we consider UFM_+ with $\mathcal{L}_{\text{SCL}}(\mathbf{H})$ being the full-batch SCL defined as,

$$\mathcal{L}_{\text{full}}(\mathbf{H}) := \sum_{i \in [n]} \frac{1}{n_{y_i} - 1} \sum_{j \neq i, y_j = y_i} \log \left(\sum_{\ell \neq i} \exp \left(\mathbf{h}_i^\top \mathbf{h}_\ell - \mathbf{h}_i^\top \mathbf{h}_j \right) \right). \quad (2)$$

Thm. 1 specifies the optimal cost and optimizers of UFM_+ with the full-batch SCL (2).

Theorem 1 (Full-batch SCL minimizers). *Let $d \geq k$. For any \mathbf{H} feasible in UFM_+ , the following lower bound holds,*

$$\mathcal{L}_{\text{full}}(\mathbf{H}) \geq \sum_{c \in [k]} n_c \log \left(n_c - 1 + (n - n_c)e^{-1} \right). \quad (3)$$

Moreover, equality is achieved if and only if \mathbf{H} satisfies NC and the class-means form a k -OF.

⁴[TB22] has also studied incorporating the ReLU activation in the UFM, albeit focusing on MSE loss.

Remark 2. The normalization of the embeddings in UFM_+ corresponds to SCL with temperature $\tau = 1$. More generally, the normalization becomes $\|\mathbf{h}_i\|^2 = 1/\tau$. The conclusion of Thm. 1 is insensitive to the choice of τ , thus stated above for $\tau = 1$ without loss of generality. Although the value of τ does not affect the global optimizers of UFM_+ , we have empirically observed that it impacts the speed of convergence during training.

We defer the details of the proof to Sec. A in the appendix. The bound relies on successive uses of Jensen’s inequality and the fact that for feasible \mathbf{H} , each pair of training samples $i, j \in [n]$ satisfies $0 \leq \mathbf{h}_i^\top \mathbf{h}_j \leq 1$. We complete the proof by verifying that equality is attained only if $\mathbf{h}_i^\top \mathbf{h}_j = 1$ when $y_i = y_j$ and $\mathbf{h}_i^\top \mathbf{h}_j = 0$ when $y_i \neq y_j$. In other words, to achieve the optimal cost, the features with similar labels must align (NC) and the class-mean features should form an OF.

Thm. 1 shows that any optimal embedding geometry learned by the full-batch SCL with ReLU constraints uniquely follows the OF geometry (Defn. 3) and the conclusion is independent of the training label distribution. We have already seen in Sec. 3, that this conclusion is empirically verified by deep-net experiments. To further verify the lower bound on the cost of the SCL loss given by the theorem, we compare it in Fig. 4 with the empirical loss of a ResNet-18 model trained with full-batch SCL (2) on R -STEP MNIST dataset and $n = 1000$ total examples. Note the remarkable convergence of the loss to the lower bound (dashed horizontal lines) as training progresses.

4.2 Mini-batch SCL

Thm. 1 shows that minimizing SCL over the training set as a single batch recovers an OF in the feature space, regardless of the training label distribution. However, in practice, SCL optimization is performed over batches chosen from training set [Kho+20; Gra+21]. Specifically, we have a set of batches \mathcal{B} and we compute the loss on each batch $B \in \mathcal{B}$ as in (1). While in the full-batch SCL (2), all pairs of training samples interact with each other, in the mini-batch version, two samples (i, j) interact only if there exists a batch $B \in \mathcal{B}$ such that $i, j \in B$. The natural question is whether the mini-batch construction impacts the embeddings learned by SCL. In this section, we study the role of batching on the embeddings geometry more closely.

Similar to the previous section, we consider UFM_+ , where we directly optimize the SCL over embeddings \mathbf{H} . However, this time we study the mini-batch SCL defined as follows,

$$\mathcal{L}_{\text{batch}}(\mathbf{H}) := \sum_{B \in \mathcal{B}} \sum_{i \in B} \frac{1}{n_{B, y_i} - 1} \sum_{\substack{j \in B \\ j \neq i, y_j = y_i}} \log \left(\sum_{\substack{\ell \in B \\ \ell \neq i}} \exp(\mathbf{h}_i^\top \mathbf{h}_\ell - \mathbf{h}_i^\top \mathbf{h}_j) \right), \quad (4)$$

where recall $n_{B, c} = |\{i : i \in B, y_i = c\}|$. The following theorem is an extension of Thm. 1 for the mini-batch SCL (4). The proof proceeds similarly to that of Thm. 1, where the loss over each batch can be independently bounded from below. Interestingly, due to the orthogonality of the optimal embeddings in every batch, the lower bound for each batch can be achieved by the common minimizer. The detailed proof is deferred to Sec. B in the appendix.

Theorem 2 (Mini-batch SCL minimizers). *Let $d \geq k$ and \mathcal{B} be an arbitrary set of batches of examples. For any feasible \mathbf{H} in UFM_+ , the following lower bound holds,*

$$\mathcal{L}_{\text{batch}}(\mathbf{H}) \geq \sum_{B \in \mathcal{B}} \sum_{c \in [k]} n_{B, c} \log(n_{B, c} - 1 + (n_B - n_{B, c})e^{-1}). \quad (5)$$

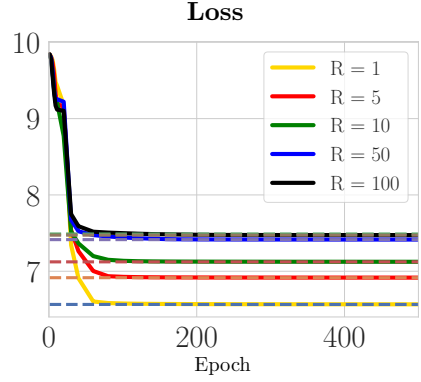


Figure 4: Full-batch SCL converges to the lower bound (dashed lines) computed in Thm. 1 during training. See text for details.

Moreover, equality holds if and only if for every $B \in \mathcal{B}$ and every pair of samples $i, j \in B$, $\mathbf{h}_i^\top \mathbf{h}_j = 0$ if $y_i \neq y_j$ and $\mathbf{h}_i = \mathbf{h}_j$ if $y_i = y_j$.

Global minimizer geometry may not be unique. It is easy to verify that any \mathbf{H} following the OF geometry achieves the lower-bound and it is also a global optimizer of the mini-batch SCL. However, depending on the choice of \mathcal{B} , the lower bound can possibly be attained by other optimal embeddings that do not necessarily satisfy NC or orthogonality. Hence the global optimizer may not have a unique geometry.

To highlight the importance of \mathcal{B} in the characterization of the optimal geometry of UFM_+ when using the batch-loss, consider the toy example in Fig. 5. Suppose we have $k = 3$ classes and we want to find the optimal normalized and non-negative features in \mathbb{R}^3 by minimizing (4) for $\mathcal{B} = \{B_1, B_2\}$. Although the OF satisfies the global optimality condition in Thm. 2, the theorem requires milder conditions for the optimal $\widehat{\mathbf{H}}$: $\widehat{\mathbf{h}}_i$ and $\widehat{\mathbf{h}}_j$ need to be aligned ($y_i = y_j$) or orthogonal ($y_i \neq y_j$) only if they interact within one of the selected batches. Fig. 5 shows one such optimal geometry that does not satisfy either of NC or orthogonality conditions: Firstly, the samples $i = 1$ and $i = 3$ have significantly different features despite belonging to the same class. Second, $\widehat{\mathbf{h}}_3, \widehat{\mathbf{h}}_4$ align with $\widehat{\mathbf{h}}_5, \widehat{\mathbf{h}}_6$ although they have different labels, and $\widehat{\mathbf{h}}_7, \widehat{\mathbf{h}}_8$ are not orthogonal to samples $\widehat{\mathbf{h}}_1, \widehat{\mathbf{h}}_2$. With this example, we are now ready to discuss the role of batching more formally in the next section.

5 Batching matters

By the fact that the OF geometry may not be the unique solution for the UFM_+ with mini-batch SCL (4), here we study the role of mini-batches for optimizing SCL to avoid ambiguous solutions with different geometries. In Sec. 5.1, we first identify necessary and sufficient conditions for a batching strategy to yield a unique solution geometry to the global minimizers. Then, in Sec. 5.2, using this result, we propose a simple yet effective scheme that provably succeeds in improving the convergence to an OF.

5.1 When is OF geometry the unique minimizer?

As discussed in Sec. 4.2 the uniqueness of the global minimizer's geometry when considering mini-batches depends on the interaction of samples in the loss function, or, in other words, the choice of \mathcal{B} . Before specifying for which \mathcal{B} the minimizer is unique, we need to define the Batch Interaction Graph, a graph that captures the pairwise interactions of samples within the batches.

Definition 4 (Batch Interaction Graph). *Consider an undirected graph $G = (V, E)$ where $V := [n]$. We define the Batch Interaction Graph for a given set of batches \mathcal{B} as follows: vertices $u, v \in V$ are connected if and only if there exists a batch $B \in \mathcal{B}$ such that $u, v \in B$. Moreover, G_c denotes the induced subgraph of G with vertices $V_c = \{u : y_u = c\}$.*

With this definition, we can now state the necessary and sufficient conditions on \mathcal{B} for the minimizer of the mini-batch SCL to be uniquely OF.

Corollary 2.1. *Consider the Batch Interaction Graph G corresponding to \mathcal{B} . The global optimizer of UFM_+ with mini-batch SCL (4) is unique and forms an OF if and only if G satisfies*

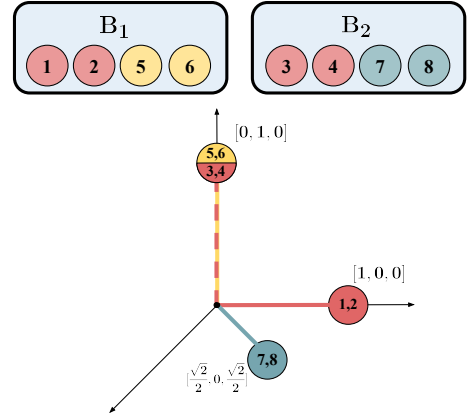


Figure 5: A non-OF optimal feature geometry minimizing the mini-batch SCL (4) with $\mathcal{B} = \{B_1, B_2\}$. Samples with different labels are marked with different colors. See text for details.

either of NC or orthogonality conditions: Firstly, the samples $i = 1$ and $i = 3$ have significantly different features despite belonging to the same class. Second, $\widehat{\mathbf{h}}_3, \widehat{\mathbf{h}}_4$ align with $\widehat{\mathbf{h}}_5, \widehat{\mathbf{h}}_6$ although they have different labels, and $\widehat{\mathbf{h}}_7, \widehat{\mathbf{h}}_8$ are not orthogonal to samples $\widehat{\mathbf{h}}_1, \widehat{\mathbf{h}}_2$. With this example, we are now ready to discuss the role of batching more formally in the next section.

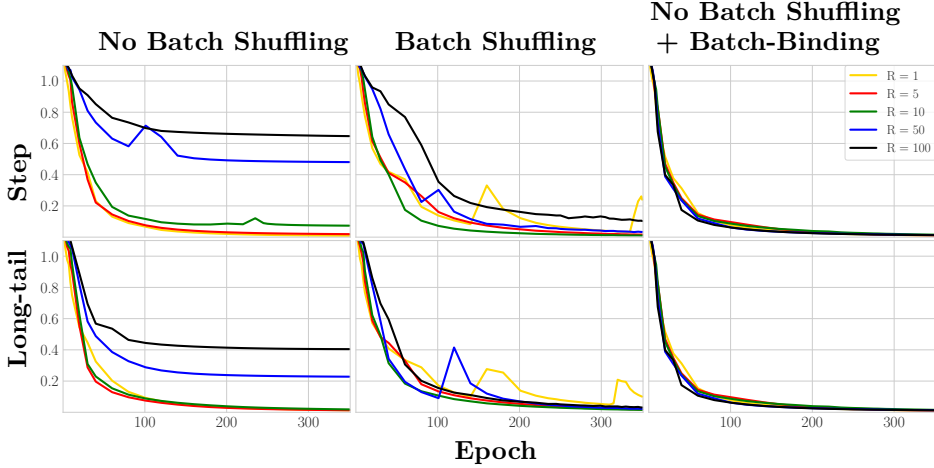


Figure 6: Convergence to the OF geometry for various batching schemes including the analysis-inspired scheme “No Batch Shuffling + Batch-Binding”. See text for details. Experiments conducted with CIFAR-10 and ResNet-18.

the following conditions: (1) For every class $c \in [k]$, G_c is a connected graph. (2) For every pair $c_1, c_2 \in [k]$, there exists at least one edge between G_{c_1} and G_{c_2} .

Corollary 2.1 serves as a check to ascertain whether a given batching scheme yields a unique global minimizer geometry or not. It also provides guidance for designing mini-batches. We elaborate on this aspect in the following section.

5.2 Batch-binding improves convergence

Corollary 2.1 shows that an arbitrary set of mini-batches is not guaranteed to have OF geometry as its minimizing configuration in the embedding space. To enforce the OF geometry as the unique minimizer, we introduce a simple scheme with low computational overhead as follows.

Algorithm 1 Batch-binding

```

1: procedure BATCH-BINDING(a set of mini-batches  $\mathcal{B}$ , number of classes  $k$ )
2:   Binding examples: A set of examples represents a set of binding examples if it includes
      exactly one example from every class. This set has, thus,  $k$  elements.
3:   To every batch  $B \in \mathcal{B}$  add the chosen set of binding examples to create a new batch
      configuration  $\mathcal{B}'$ 
4: end procedure

```

Algorithm 1 increases the size of every mini-batch by a constant value k . This value is typically smaller than the batch sizes used to train SCL which could range from 2048 to 6144 [Kho+20]. While adding small computational overhead, this method guarantees that \mathcal{B}' satisfies the conditions of Cor. 2.1 and SCL learns an OF geometry. We conduct a series of experiments to illustrate the impact of batch binding on convergence to OF.

Geometry convergence for different batching schemes. To verify the role of batch selection on the learned features, we train ResNet-18 on CIFAR-10 under three batching scenarios: 1) **No batch-shuffling**: a mini-batch set \mathcal{B} that partitions the training examples once at initialization and is held constant across training epochs. 2) **Batch-shuffling**: the examples are divided into mini-batch partition, with a random reshuffle of the examples at *every* epoch. 3) **No batch-shuffling + batch-binding**: we construct a fixed partition of examples into mini-batches. Further, to each mini-batch we append a fixed set of k binding examples. This remains constant throughout the training.

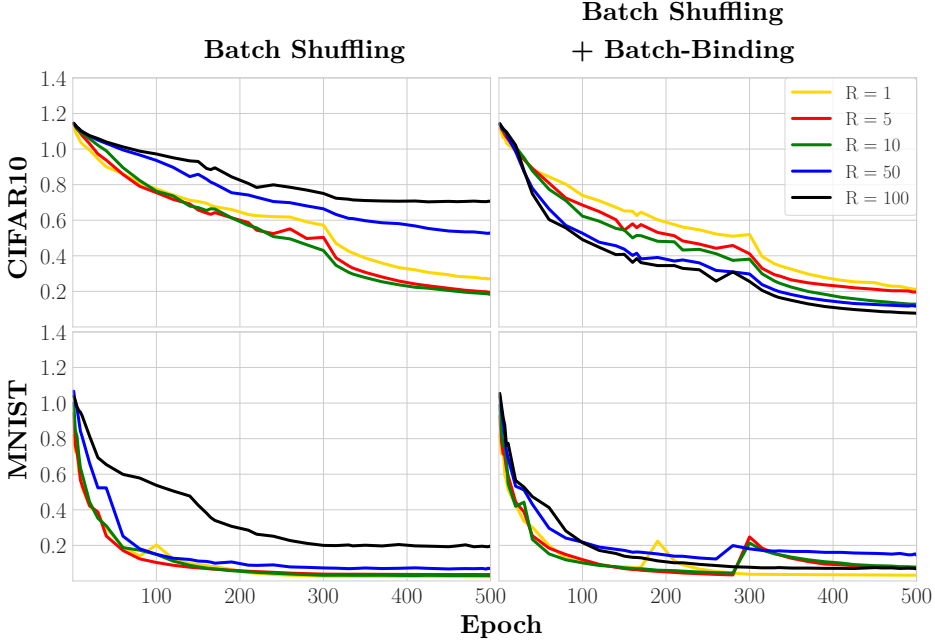


Figure 7: Convergence of \mathbf{G}_M to the OF geometry for a DenseNet-40 model trained on CIFAR10 and MNIST under STEP imbalance with and without batch-binding. While the impact of batch-bindings is less noticeable when training on a simple dataset such as MNIST, the convergence is significantly improved, particularly under imbalance, when training on a more complex dataset such as CIFAR10.

Fig. 6 shows the distance of learned embeddings to the OF geometry for the three batching scenarios mentioned above. In case of the fixed partition batching (left), the features do not converge to OF, especially with large imbalance ratios. This behavior is consistent with the conditions identified by Thm. 2, because in a typical random partition, the corresponding induced subgraphs are not necessarily connected. On the other hand, when the batching is performed with a randomly reshuffled data ordering (center), the geometry converges more closely to the OF, albeit with certain epochs deviating significantly from the convergence direction. We hypothesize that random reshuffling creates an opportunity for different examples to interact sufficiently, thus, when trained long enough, to converge close to an OF geometry.

Finally, with the third batching strategy (right), by adding the binding examples to the batches, even without shuffling the samples at every epoch, we observe a consistently fast convergence to the global optimizer, OF. These observations provide strong evidence supporting our analysis of batching predicting the behavior of SCL trained deep-nets. Moreover, in Table 1 in the appendix, we present experimental evidence in suggesting that batch binding does not negatively effect the balanced test accuracy of *Nearest Class Center* (NCC) classifier. This observation, paired with the impact of binding examples on OF convergence, motivates further analysis of the relationship between OF geometry and test accuracy.

Improving convergence for less powerful models. When conducting our experiments for Fig. 1, we have noticed that DenseNet-40 converges slower compared to ResNet-18. A reason for this may be related to the very different complexities of the two models: ResNet-18 has substantially more trainable parameters compared to DenseNet-40. In an attempt to improve the convergence speed, we reduce the batch size for DenseNet experiments to 128 to increase the number of SGD iterations. We also train DenseNet for 500 epochs instead of 350 while reducing the learning rate from 0.1 to 0.01 at epoch 300. Yet, we observe that with much smaller batch sizes, the embedding geometry does not always converge to the OF geometry, especially when training with high imbalance ratios. Specifically when training with randomly reshuffled batches, there is a higher chance that the examples do not interact with each other even if trained for

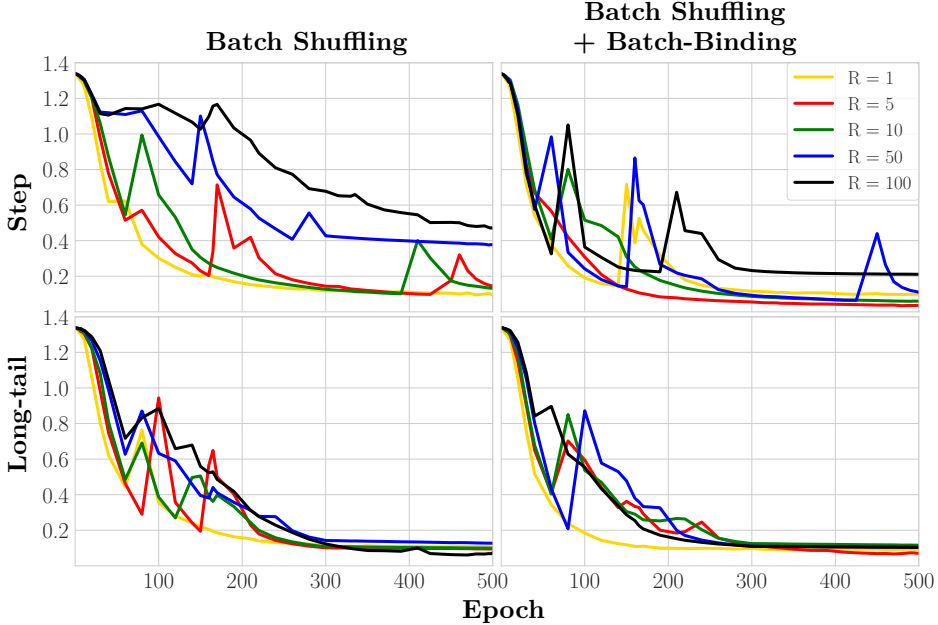


Figure 8: Convergence of embeddings geometry to OF as measured by $\Delta_{\mathbf{G}_M} := \left\| \frac{\mathbf{G}_M}{\|\mathbf{G}_M\|_F} - \frac{\mathbf{I}_k}{\|\mathbf{I}_k\|_F} \right\|_F$ for ResNet-18 trained on imbalanced CIFAR100 with SCL and different batching schemes. Adding binding examples helps with the convergence to the OF geometry, especially under STEP imbalance with larger imbalance ratios.

long, suggesting that the optimal solution for all batches is not necessarily OF. We hypothesize that this likelihood increases when using smaller batch sizes during training. In order to combat this effect, we ran the DenseNet experiments with the addition of binding examples to every batch. As shown in Fig. 7, we find that adding such binding examples significantly improves the convergence to OF, particularly when training on more complex datasets (CIFAR10 compared to MNIST) and under more severe imbalances (STEP imbalance with $R = 50, 100$). These results emphasize the impact of batch-binding and provide further evidence regarding our claims in Sec. 4.2. While the convergence values of $\Delta_{\mathbf{G}_M}$ are higher when compared to ResNet-18, we deem them reasonable considering the difference in the number of parameters between the two architectures. Similar to ResNet-18, we provide geometric convergence results for DenseNet-40 on different datasets in Fig. 19 in the appendix.

Improving convergence for more complex datasets. In addition to the benchmark datasets previously explored, we consider the convergence of ResNet-18 embeddings to the OF geometry when trained with CIFAR100. The models are trained for 500 epochs with a constant learning rate of 0.1 and a batch size of 1024. With a large number of classes ($k = 100$ for CIFAR100), it becomes increasingly more likely for the randomly reshuffled batches to not allow sufficient interactions between examples. Particularly for large imbalance ratios (e.g., $R = 100, 50$), since the number of samples in each minority class could become as low as 5-10, some batches might never encounter examples from minority classes. However, including the binding examples in each batch can improve the convergence of the feature geometry to OF. In Fig. 8 we measure the convergence of ResNet-18 trained both with and without the batch-binding. Batch-binding considerably expedites and improves the convergence to the OF. This is particularly noticeable for STEP-Imbalance and large imbalance ratios, where half of the classes are minorities, thus the inclusion of binding examples becomes crucial in ensuring that our theoretical requirements for reaching the OF are satisfied.

On the convergence of batch-shuffling to OF. It can be readily observed that a fixed mini-batch partition without shuffling (*No batch-shuffling* in the experiments above) does not satisfy the conditions of Cor. 2.1. Consequently, OF is *not* the unique minimizer geometry in

such scenarios. This is clearly manifested by the inadequate convergence levels observed in our experiments, as depicted for example in Fig. 6. In contrast, in our experiments, when the examples are randomly shuffled prior to partitioning into mini-batches at each epoch (which we call *Batch Shuffling*), the convergence behavior to OF shows a significant improvement compared to the case of *No batch-shuffling*. The observed improvement can be attributed to the fact that shuffling enables interactions among examples across epochs. To elaborate on this notion, we present a formalization of batch shuffling below.

Let \mathcal{S} denote the set of all permutations of $[n] = \{1, 2, \dots, n\}$, where n is the total number of training examples. Additionally, let b denote a fixed batch-size. For simplicity, assume n is an integer multiple of b . At the beginning of each training epoch t , we sample a permutation $s_t = (i_1, i_2, \dots, i_n)$ uniformly from \mathcal{S} with replacement. We then define $\mathcal{P}(s_t) := \{\{i_1, \dots, i_b\}, \{i_{b+1}, \dots, i_{2b}\}, \dots, \{i_{n-b+1}, \dots, i_n\}\}$ as the collection of total $\frac{n}{b}$ mini-batches obtained by partitioning s_t . These are the mini-batches used at epoch t . Thus, SCL in this epoch can be written as follows:

$$\mathcal{L}_{s_t}(\mathbf{H}) := \sum_{B \in \mathcal{P}(s_t)} \sum_{i \in B} \mathcal{L}_B(\mathbf{H}; i), \quad \text{where } \mathcal{L}_B(\mathbf{H}; i) := \frac{1}{n_{B, y_i} - 1} \sum_{\substack{j \in B \\ j \neq i, y_j = y_i}} \log \left(\sum_{\ell \in B \setminus \{i\}} \exp(\mathbf{h}_i^\top \mathbf{h}_\ell - \mathbf{h}_i^\top \mathbf{h}_j) \right),$$

and recall $n_{B, c} = |\{i : i \in B, y_i = c\}|$. Consider also the loss over *all* mini-batches obtained by partitioning each permutation of \mathcal{S} :

$$\mathcal{L}_{\mathcal{S}}(\mathbf{H}) := \sum_{s \in \mathcal{S}} \sum_{B \in \mathcal{P}(s)} \sum_{i \in B} \mathcal{L}_B(\mathbf{H}; i), \quad (6)$$

Now, since s_t is uniformly sampled from \mathcal{S} , we have the following relation for the expected per-epoch loss to the total loss given in Eqn. (6): $\mathbb{E}_{s_t} \mathcal{L}_{s_t}(\mathbf{H}) = 1/|\mathcal{S}| \mathcal{L}_{\mathcal{S}}(\mathbf{H})$. Therefore, training with batch-shuffling can be regarded as a stochastic version of minimizing the total loss in Eq. (6). Regarding the latter, it can be checked (see Rem. 3 below) that it satisfies the conditions of Cor. 2.1, thereby making OF its unique minimizer geometry. Taken together, these findings suggest that although the per-epoch loss \mathcal{L}_{s_t} obtained through batch-shuffling does not satisfy the conditions of Cor. 2.1 for any specific epoch t , it does satisfy them in expectation. In particular, this can be regarded as preliminary justification of the experimental observation of improved convergence with *batch-shuffling* compared to *No batch-shuffling* schemes. The latter schemes fail to satisfy Cor. 2.1 under any circumstances, unless in the extreme case of a large batch size where $b = n$ and we recover $\mathcal{L}_{\text{full}}$. However, it is important to note that the aforementioned argument is a rough approximation, as it is not feasible to average over all $|\mathcal{S}| = n!$ permutations when optimization is typically performed over a limited number of epochs. This can explain why, despite exhibiting better convergence compared to the No batch-shuffling schemes, batch-shuffling schemes still demonstrate non-smooth and inconsistent convergence patterns in our experiments. This behavior becomes particularly evident when comparing the convergence levels of batch-shuffling to our *batch-binding* scheme, which is specifically designed to satisfy the conditions of Cor. 2.1 at *each* epoch.

Remark 3. *To show that Eqn. (6) satisfies Cor. 2.1, we will show that the corresponding batch interaction graph G is a complete graph. This suffices, because the induced subgraphs G_c from Def. 4 for a complete graph are connected graphs, and there exist multiple edges between G_{c_1} and G_{c_2} for $c_1, c_2 \in [k]$. To show that G is a complete graph, we argue as follows. Consider the set \mathcal{B} of all mini-batches obtained by partitioning all $n!$ elements of \mathcal{S} . Fix $b \geq 2$, so that the mini-batches have at least two examples. We will consider a subset $\mathcal{B}_1 \subseteq \mathcal{B}$ of mini-batches and show that the corresponding batch interaction graph for \mathcal{B}_1 is a complete graph, which would then imply the batch interaction graph of \mathcal{B} is also a complete graph. Specifically, let $\mathcal{B}_1 \subseteq \mathcal{B}$ denote the mini-batches comprising of the first b indices in every permutation $s \in \mathcal{S}$. In other words, from a given $s = (i_1, i_2, \dots, i_n) \in \mathcal{S}$, we let \mathcal{B}_1 include the mini-batch $\{i_1, i_2, \dots, i_b\}$. Since \mathcal{S}*

includes all permutations of $[n]$, \mathcal{B}_1 contains all b -length permutations of the elements of $[n]$, possibly with repetitions. Thus, the batch interaction graph created by the mini-batches in \mathcal{B}_1 is a complete graph. In the definition of the batch interaction graph, since a repeated presence of a pair of examples does not alter the graph, the batch interaction graph for \mathcal{B} is the same complete graph. Thus, \mathcal{B} satisfies Cor. 2.1.

6 Discussion

6.1 More related work

The simple concept behind SCL, introduced as an extension of the contrastive loss [e.g., Che+20; TKI19] to the fully supervised setting by Khosla et al. [Kho+20], involves pulling together the normalized features of examples belonging to the same class while pushing them away from examples of other classes. Despite its simplicity, SCL offers a generalization of existing loss functions like the triplet loss [WBS05] and the N-pair loss [Soh16], and surpasses the performance of the CE loss on standard vision classification datasets [Kho+20], while also being more robust to natural corruptions in the data and less sensitive to hyperparameters. Further studies have also emphasized the observed resilience of SCL and variants alike to distribution shifts, particularly in scenarios involving training with imbalanced data [Gun+20; Jit+22; SC21; Li+22; Gun+20; Kan+21; Li+22]. These studies commonly involve training a combination of CE and SCL-type losses.

In recent years, there has been a notable increase in interest regarding the properties of the embedding space and weight vectors learned through unsupervised and supervised contrastive losses, as well as CE. Of particular importance is the endeavor to uncover the fundamental distinctions between these losses, which could be essential in order to effectively harness the respective strengths of each method and formalize principled ways to combine them. Specifically, an increasing series of recent works have focused on uncovering the embedding geometry of CE, Mean-Squared Error (MSE) losses, and their variants [PHD20; Zhu+21; Zho+22a; Zho+22b; LS20; Thr+22; Yar+22; Beh+23; Gao+23; Zho+22b; Yar+22; Gra+21; TB22; HPD21; Fan+21; SML23]. In addition to the scientific curiosity surrounding such studies, this exploration has paved the way for novel CE-based approaches to training DNNs on imbalanced data [Beh+23; LD23; Xie+23; Sha+23; Dan+23].

However, less attention has been devoted in the existing literature to a comparable set of comprehensive results for the Supervised Contrastive Learning (SCL) loss. Graf et al. [Gra+21] is the first study that explicitly delves into understanding the embedding geometry of SCL and comparing it to that of CE. While this study is pioneering, we note two limitations. Firstly, their investigation primarily focuses on balanced data. Secondly, to reconcile the theoretically predicted simplex ETF geometry with the observed experimental outcomes, they adopt a heuristic strategy involving shifting the center of the embeddings. However, this approach lacks theoretical support and does *not* result in predicting the orthogonal angle between embeddings, as depicted in Fig. 1. To tackle the first point, and inspired by suggestions in [Gra+21] that balanced data is crucial for obtaining symmetric embeddings geometries, Zhu et al. [Zhu+22] have very recently proposed and investigated a clever modification of the SCL that significantly boosts performance under class imbalances. Our work addresses the two limitations identified above in the study of [Gra+21] and complements the findings of [Zhu+22] by showing that vanilla SCL can actually learn symmetric embedding structure even in the presence of imbalances.

6.1.1 Why is batch analysis “easier” for \mathbf{UFM}_+ rather than \mathbf{UFM} ?

Graf et al. [Gra+21, Thm. 2] studies the UFM without ReLU constraints and with balanced labels, and proves that the global solution is a simplex ETF. The authors note that their proof relies on the batch construction as the set of all combinations of a given size. In contrast, we

have proved that for UFM_+ the global solution is an OF for a wider range of batching scenarios (specifically, as long as they satisfy the interaction properties characterized in Cor. 2.1). Without ReLU, as noted by Graf et al. [Gra+21, Fig. 5], the optimal configuration of examples in each batch can have a different geometry, depending on the label distribution of the examples within the batch. However, *with* ReLU, the optimal configuration of every batch is an OF over the classes whose examples are present in the batch. In particular, there is no contradiction between two mini-batches having both overlapping and mutually exclusive classes, since the optimal configuration of one batch does not violate the optimal configuration of another. Furthermore, the overall batch construction can have a unique OF as the optimal configuration provided the conditions in Cor. 2.1 are satisfied. The conditions include the batching assumed by Graf et al. [Gra+21] as a special case, while being applicable in less restrictive scenarios. Sec. 5.2 explored the implications of this finding, by studying the criteria for a batching scheme to lead to a unique minimizer geometry and further suggesting a simple scheme to convert an arbitrary batching to one satisfying these criteria.

6.2 Detailed comparison between UFM and UFM_+

Within this section, we provide an in-depth analysis, expanding upon our earlier discussions, of the disparities between the predictions generated by the UFM, commonly utilized in previous studies, and the refined version UFM_+ that we employ in this work to study the embedding geometry of SCL.

The majority of previous works [e.g., PHD20; Zhu+21; Fan+21] study the geometry of learned embeddings by investigating a proxy unconstrained features model (UFM). Specifically, the UFM drops the dependence of the learned embeddings \mathbf{H} on the network parameters $\boldsymbol{\theta}$, and finds optimal $\widehat{\mathbf{H}}$ that minimizes the loss function. In case of SCL, as studied in e.g., [Gra+21], the corresponding UFM is as follows,

$$\arg \min_{\mathbf{H}} \mathcal{L}_{\text{SCL}}(\mathbf{H}) \text{ subj. to } \|\mathbf{h}_i\|^2 = 1, \forall i \in [n]. \quad (\text{UFM})$$

As explained in Sec. 4, this paper employs a refined version of the UFM, namely UFM_+ , to characterize the representations learned by SCL. Specifically, UFM_+ further constrains the embeddings \mathbf{H} to be non-negative, in this way accounting for the ReLU activation commonly used in several deep-net architectures. Thus the search for the optimal \mathbf{H} is restricted to the non-negative orthant.

6.2.1 Centering heuristic

Many deep neural network models incorporate ReLU activations, resulting in nonnegative feature embeddings at the last layer. In contrast, the UFM does not impose any constraints on the optimal \mathbf{H} , allowing it to contain negative entries. To bridge this gap, previous works [e.g., PHD20; Zhu+21; Fan+21; Zho+22a; Thr+22; Zho+22b] apply a heuristic approach called *global-mean centering* on the learned embeddings before comparing their arrangement with the theoretical prediction given by the UFM. Specifically, the centering heuristic is applied as follows: Prior to comparing the geometries, we subtract the global-mean embedding $\boldsymbol{\mu}_G = \frac{1}{k} \sum_{c \in [k]} \boldsymbol{\mu}_c$ from all class-mean embeddings $\boldsymbol{\mu}_c$ to form the *centered class-mean embeddings* $\bar{\boldsymbol{\mu}}_c$:

$$\bar{\boldsymbol{\mu}}_c = \boldsymbol{\mu}_c - \boldsymbol{\mu}_G, \quad \bar{\mathbf{M}} = [\bar{\boldsymbol{\mu}}_1 \ \cdots \ \bar{\boldsymbol{\mu}}_k].$$

Indeed, this heuristic centering operation effectively ensures that the mean-embedding matrix $\bar{\mathbf{M}}$, after the necessary shifting, is centered at the origin, satisfying $\bar{\mathbf{M}}\mathbf{1}_k = 0$. This property also holds for the global optimizers of the UFM found in the previous work, which served as a motivation for the heuristic centering.

Unlike the approach mentioned above, our findings do not necessitate any heuristic embedding processing for comparing the geometries. This is because our model directly provides the geometry of the embeddings in their original form.

6.2.2 Centered OF is simplex ETF

Focusing on the SCL, Graf et al. [Gra+21] have used the **UFM** to characterize the learned embeddings and have found that, for balanced classes, the simplex ETF geometry is the global optimizer of **UFM**. In other words, the optimal embeddings \mathbf{H} adhere to the NC (Defn. 1), and the corresponding mean embeddings \mathbf{M} form a simplex ETF. For the reader’s convenience, we recall below the definition of simplex ETF from [PHD20].

Definition 5 (Simplex ETF). *We say that k vectors $\mathbf{V} = [\mathbf{v}_1, \dots, \mathbf{v}_k] \in \mathbb{R}^{d \times k}$ form a simplex-ETF if $\mathbf{V}^\top \mathbf{V} \propto \mathbb{I}_k - \frac{1}{k} \mathbf{1}_k \mathbf{1}_k^\top$, i.e., for each pair of $(i, j) \in [k]$, $\|\mathbf{v}_i\| = \|\mathbf{v}_j\|$ and $\frac{\mathbf{v}_i^\top \mathbf{v}_j}{\|\mathbf{v}_i\| \|\mathbf{v}_j\|} = \frac{-1}{k-1}$.*

In this paper, we show instead that the global optimizer of **UFM** is an OF. Remarkably, this result holds true regardless of the label-imbalance profile. However, for the purpose of comparison with the findings of [Gra+21], let’s specifically consider the scenario of balanced data. In this case, an intriguing question arises:

Specifically for balanced data, how does our discovery that embeddings converge to an OF compare to the previous finding by [Gra+21] that embeddings converge to an ETF?

The answer to this question lies on the centering trick discussed in Section 6.2.1. Specifically, stating that embeddings form an OF implies that *centered* embeddings form an ETF. This straightforward fact is formalized in the following lemma.

Lemma 6.1. *Suppose that a set of vectors $\{\mathbf{v}_1, \dots, \mathbf{v}_k\}$ form a k -OF in \mathbb{R}^d with $d \geq k$, and their mean-centered counterparts are $\bar{\mathbf{v}}_c = \mathbf{v}_c - \mathbf{v}_G, \forall c \in [k]$, where $\mathbf{v}_G = \frac{1}{k} \sum_{c \in [k]} \mathbf{v}_c$. Then, the centered embeddings $\{\bar{\mathbf{v}}_1, \dots, \bar{\mathbf{v}}_k\}$ form a simplex ETF spanning a $k-1$ -dimensional subspace.*

Lemma 6.1 states that based on our finding that embeddings form an OF, we can deduce that centered embeddings form an ETF. This conclusion aligns with the analysis conducted by [Gra+21] on the UFM. However, the UFM analysis itself does not provide information regarding the necessity of the centering technique, which remains heuristic. Additionally, it is important to note that it is unclear how to establish that (uncentered) embeddings form an OF if we initially know that centered embeddings form an ETF. This is due to the unknown vector used for centering, which cannot be determined. This issue of identifiability is the underlying reason why the angle prediction eventually made by [Gra+21] in Fig. 1 deviates from the true value of ninety degrees, which corresponds to the OF.

6.2.3 UFM can fail to predict the true geometry

In the previous section, we demonstrated that for balanced data, the solution found by the **UFM** does not predict the true geometry of the embeddings (i.e., OF), but it can predict the

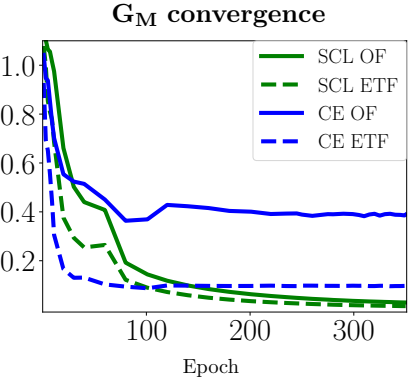


Figure 9: Comparing the convergence of embeddings geometries for SCL (in green) and CE (in blue) on balanced CIFAR10 with ResNet-18. Solid lines track the distance of *uncentered* embeddings to OF and dashed lines track the distance of *centered* embeddings to simplex ETF. For CE, the learning rate and weight decay and batch size are set according to [PHD20]. Note the convergence of SCL (solid green) to its implicit geometry is noticeably better compared to CE (dashed blue).

geometry of the embeddings after the application of a global-mean centering heuristic (i.e., ETF). Naturally this raises the following question:

Does the UFM consistently provide accurate predictions for the geometry of the centered embeddings? In other words, does the OF geometry predicted by our refined UFM_+ always align with being a global optimizer of the UFM after centering?

The lemma presented below demonstrates that the answer to this question is negative. Specifically, it shows that the global optimizer of UFM is sensitive to the label distribution of the training set, thus ETF is not necessarily a global optimizer in the presence of imbalances. This is in contrast to UFM_+ , for which we showed that the global optimizer is consistently an OF, irrespective of the labels distribution. In other words, the difference between UFM and UFM_+ cannot be addressed by only considering the centering of the optimal embeddings in general.

Lemma 6.2. *If classes in the training set are not balanced, the global solution of UFM is not necessarily an ETF. Thus, the solution of UFM_+ (which according to Thm. 1 is an OF) is in general different to that of UFM even after centering is applied.*

Remark 4. *While Zhu et al. [Zhu+22] acknowledge that the global optima of the UFM do not conform to the ETF geometry in the presence of class imbalance, they do not provide a formal proof to support this claim. In this context, Lemma 6.2 fulfills this purpose.*

6.3 Comparing implicit Geometries: SCL vs CE – A summary

We conclude this discussion by providing a summary of the observations on the contrasting implicit geometries of embeddings between the two loss functions: SCL and CE.

1. The SCL geometry is robust to label-imbalances. Specifically, the geometry of SCL embeddings exhibits symmetry consistently, whereas imbalances introduce distortions in the implicit geometry of CE embeddings [Fan+21; Thr+22].

2. The convergence of SCL to its implicit geometry is notably superior. The measured geometry of SCL exhibits a faster decrease in distance from its analytic formula (i.e., OF) with each epoch, eventually reaching lower values. This holds true not only for label-imbalanced data, where [Thr+22] finds that the convergence of embeddings deteriorates as the imbalance ratio increases, but also for balanced data, where the convergence of embeddings with CE is inferior compared to classifiers [PHD20]; see Fig. 9 for visualization.

3. For SCL, batching matters. During CE training, when using any arbitrary batching method, there exists an implicit interaction among all the examples, that is facilitated by the inclusion of the classifier vectors in the loss objective. On the other hand, with SCL, the interactions between examples are explicitly controlled by the mini-batches. Specifically, our analysis of the role of batches in Secs. 4.2 and 5.1, along with the batch-binding scheme presented in Sec. 5.2 reveal that the structure of mini-batches critically affects the geometry of the learnt embeddings.

7 Concluding remarks

We have shown consistent empirical and theoretical evidence that SCL learns training embeddings that converge to the OF geometry irrespective of the level of class imbalance. We believe this finding contributes a unique result to the growing literature of neural-collapse / implicit-geometry phenomena. For balanced data, our results demystify the heuristic centering of the theoretical ETF geometry, as implemented by Graf et al. [Gra+21] in their attempt to match experiments where embeddings are non-negative. For imbalanced data, our results stand as the first explicit characterization of the geometry, dispelling suspicions that imbalances alter the geometry [Zhu+22]. In both cases, these advancements are achieved by analyzing a refined UFM model, UFM_+ , that closely aligns with experimental conditions by constraining embeddings to the

non-negative orthant. The refined model also leads to new findings about the intricate role of batching in SCL optimization, that may be of independent interest. However, like many studies on neural-collapse phenomena, our results also have a common limitation. They only provide insights into the behavior of deep neural networks during training. On the other hand, there is a related line of recent research that explores algorithmic modifications to SCL [Gun+20; Jit+22; SC21; Li+22; Gun+20; Kan+21; Li+22], often rooted but not explicitly connected to geometric principles alike, to enhance generalization under imbalances. Ultimately, we envision the two research streams merging through the ongoing exchange of ideas.

References

- [Beh+23] Tina Behnia, Ganesh Ramachandra Kini, Vala Vakilian, and Christos Thrampoulidis. “On the Implicit Geometry of Cross-Entropy Parameterizations for Label-Imbalanced Data”. In: *International Conference on Artificial Intelligence and Statistics*. PMLR. 2023, pp. 10815–10838.
- [Che+20] Ting Chen, Simon Kornblith, Mohammad Norouzi, and Geoffrey Hinton. “A simple framework for contrastive learning of visual representations”. In: *International conference on machine learning*. PMLR. 2020, pp. 1597–1607.
- [Dan+23] Hien Dang, Tan Nguyen, Tho Tran, Hung Tran, and Nhat Ho. “Neural Collapse in Deep Linear Network: From Balanced to Imbalanced Data”. In: *arXiv preprint arXiv:2301.00437* (2023).
- [Fan+21] Cong Fang, Hangfeng He, Qi Long, and Weijie J Su. “Exploring deep neural networks via layer-peeled model: Minority collapse in imbalanced training”. In: *Proceedings of the National Academy of Sciences* 118.43 (2021).
- [Gao+23] Peifeng Gao, Qianqian Xu, Peisong Wen, Huiyang Shao, Zhiyong Yang, and Qingming Huang. “A Study of Neural Collapse Phenomenon: Grassmannian Frame, Symmetry, Generalization”. In: *arXiv preprint arXiv:2304.08914* (2023).
- [Gra+21] Florian Graf, Christoph Hofer, Marc Niethammer, and Roland Kwitt. “Dissecting supervised contrastive learning”. In: *International Conference on Machine Learning*. PMLR. 2021, pp. 3821–3830.
- [Gun+20] Beliz Gunel, Jingfei Du, Alexis Conneau, and Ves Stoyanov. “Supervised contrastive learning for pre-trained language model fine-tuning”. In: *arXiv preprint arXiv:2011.01403* (2020).
- [HPD21] XY Han, Vardan Papyan, and David L Donoho. “Neural collapse under mse loss: Proximity to and dynamics on the central path”. In: *arXiv preprint arXiv:2106.02073* (2021).
- [Ji+21] Wenlong Ji, Yiping Lu, Yiliang Zhang, Zhun Deng, and Weijie J Su. “An unconstrained layer-peeled perspective on neural collapse”. In: *arXiv preprint arXiv:2110.02796* (2021).
- [Jit+22] Wittawat Jitkrittum, Aditya Krishna Menon, Ankit Singh Rawat, and Sanjiv Kumar. “ELM: Embedding and Logit Margins for Long-Tail Learning”. In: *arXiv preprint arXiv:2204.13208* (2022).
- [Kan+21] Bingyi Kang, Yu Li, Sa Xie, Zehuan Yuan, and Jiashi Feng. “Exploring balanced feature spaces for representation learning”. In: *International Conference on Learning Representations*. 2021.

[Kho+20] Prannay Khosla, Piotr Teterwak, Chen Wang, Aaron Sarna, Yonglong Tian, Phillip Isola, Aaron Maschinot, Ce Liu, and Dilip Krishnan. “Supervised contrastive learning”. In: *Advances in neural information processing systems* 33 (2020), pp. 18661–18673.

[LD23] Tong Liang and Jim Davis. “Inducing Neural Collapse to a Fixed Hierarchy-Aware Frame for Reducing Mistake Severity”. In: *arXiv preprint arXiv:2303.05689* (2023).

[Li+22] Tianhong Li, Peng Cao, Yuan Yuan, Lijie Fan, Yuzhe Yang, Rogerio S Feris, Piotr Indyk, and Dina Katabi. “Targeted supervised contrastive learning for long-tailed recognition”. In: *Proceedings of the IEEE/CVF Conference on Computer Vision and Pattern Recognition*. 2022, pp. 6918–6928.

[Liu+23] Xuantong Liu, Jianfeng Zhang, Tianyang Hu, He Cao, Yuan Yao, and Lujia Pan. “Inducing Neural Collapse in Deep Long-tailed Learning”. In: *International Conference on Artificial Intelligence and Statistics*. PMLR. 2023, pp. 11534–11544.

[LS20] Jianfeng Lu and Stefan Steinerberger. “Neural collapse with cross-entropy loss”. In: *arXiv preprint arXiv:2012.08465* (2020).

[MPP20] Dustin G Mixon, Hans Parshall, and Jianzong Pi. “Neural collapse with unconstrained features”. In: *arXiv preprint arXiv:2011.11619* (2020).

[PHD20] Vardan Petyan, XY Han, and David L Donoho. “Prevalence of neural collapse during the terminal phase of deep learning training”. In: *Proceedings of the National Academy of Sciences* 117.40 (2020), pp. 24652–24663.

[SC21] Dvir Samuel and Gal Chechik. “Distributional robustness loss for long-tail learning”. In: *Proceedings of the IEEE/CVF International Conference on Computer Vision*. 2021, pp. 9495–9504.

[Sha+23] Saurabh Sharma, Yongqin Xian, Ning Yu, and Ambuj Singh. “Learning Prototype Classifiers for Long-Tailed Recognition”. In: *arXiv preprint arXiv:2302.00491* (2023).

[SML23] Peter Súkeník, Marco Mondelli, and Christoph Lampert. “Deep Neural Collapse Is Provably Optimal for the Deep Unconstrained Features Model”. In: *arXiv preprint arXiv:2305.13165* (2023).

[Soh16] Kihyuk Sohn. “Improved deep metric learning with multi-class n-pair loss objective”. In: *Advances in neural information processing systems* 29 (2016).

[TB22] Tom Tirer and Joan Bruna. “Extended unconstrained features model for exploring deep neural collapse”. In: *arXiv preprint arXiv:2202.08087* (2022).

[Thr+22] Christos Thrampoulidis, Ganesh R Kini, Vala Vakilian, and Tina Behnia. “Imbalance Trouble: Revisiting Neural-Collapse Geometry”. In: *arXiv preprint arXiv:2208.05512* (2022).

[TKI19] Y Tian, D Krishnan, and P Isola. “Contrastive multiview coding. arXiv”. In: *arXiv preprint arXiv:1906.05849* (2019).

[WBS05] Kilian Q Weinberger, John Blitzer, and Lawrence Saul. “Distance metric learning for large margin nearest neighbor classification”. In: *Advances in neural information processing systems* 18 (2005).

[Xie+23] Liang Xie, Yibo Yang, Deng Cai, and Xiaofei He. “Neural collapse inspired attraction-repulsion-balanced loss for imbalanced learning”. In: *Neurocomputing* (2023).

[Yar+22] Can Yaras, Peng Wang, Zhihui Zhu, Laura Balzano, and Qing Qu. “Neural collapse with normalized features: A geometric analysis over the riemannian manifold”. In: *arXiv preprint arXiv:2209.09211* (2022).

[Zho+22a] Jinxin Zhou, Xiao Li, Tianyu Ding, Chong You, Qing Qu, and Zhihui Zhu. “On the Optimization Landscape of Neural Collapse under MSE Loss: Global Optimality with Unconstrained Features”. In: *arXiv preprint arXiv:2203.01238* (2022).

[Zho+22b] Jinxin Zhou, Chong You, Xiao Li, Kangning Liu, Sheng Liu, Qing Qu, and Zhihui Zhu. “Are All Losses Created Equal: A Neural Collapse Perspective”. In: *arXiv preprint arXiv:2210.02192* (2022).

[Zhu+21] Zhihui Zhu, Tianyu Ding, Jinxin Zhou, Xiao Li, Chong You, Jeremias Sulam, and Qing Qu. “A Geometric Analysis of Neural Collapse with Unconstrained Features”. In: *Advances in Neural Information Processing Systems* 34 (2021).

[Zhu+22] Jianggang Zhu, Zheng Wang, Jingjing Chen, Yi-Ping Phoebe Chen, and Yu-Gang Jiang. “Balanced contrastive learning for long-tailed visual recognition”. In: *Proceedings of the IEEE/CVF Conference on Computer Vision and Pattern Recognition*. 2022, pp. 6908–6917.

Contents

1	Introduction	1
1.1	Summary of contributions	3
1.2	Organization	3
2	Setup	4
3	SCL learns OF geometries: Empirical findings	5
4	Theoretical justification: SCL with non-negativity constraints	6
4.1	Full-batch SCL	6
4.2	Mini-batch SCL	7
5	Batching matters	8
5.1	When is OF geometry the unique minimizer?	8
5.2	<i>Batch-binding</i> improves convergence	9
6	Discussion	13
6.1	More related work	13
6.1.1	Why is batch analysis “easier” for UFM_+ rather than UFM ?	13
6.2	Detailed comparison between UFM and UFM_+	14
6.2.1	Centering heuristic	14
6.2.2	Centered OF is simplex ETF	15
6.2.3	UFM can fail to predict the true geometry	15
6.3	Comparing implicit Geometries: SCL vs CE – A summary	16
7	Concluding remarks	16
A	Proof of Thm. 1	21
B	Proof of Thm. 2	22
B.1	Proof of Cor. 2.1	23
C	Proofs for Section 6.2	24
C.1	Proof of Lemma 6.1	24
C.2	Proof of Lemma 6.2	24
D	Additional experimental results and discussion	25
D.1	Details on the main experimental setup	25
D.2	Additional geometric analysis	25
D.2.1	Neural Collapse	25
D.2.2	Angular convergence	25
D.2.3	Embedding heatmaps	26
D.2.4	Experiments with MLPs	27
D.3	Optimization dynamics	27
D.3.1	Loss convergence	27
D.3.2	Effect of τ	28
D.4	Complementary results and discussions on batch-binding	28
D.4.1	How batch-binding ensures a unique OF geometry	29
D.4.2	Impact of batch-binding on generalization	29

Additional Notations. While recalling the notation mentioned in Sec. 1, we note a few more below. \otimes denotes Kronecker products. We use $\mathbf{1}_m$ to denote an m -dimensional vector of all ones. For vectors/matrices with all zero entries, we simply write 0, as dimensions are easily understood from context. \mathbf{V}^\dagger its Moore-Penrose pseudoinverse. $\nabla_{\mathbf{V}} \mathcal{L} \in \mathbb{R}^{m \times n}$ is the gradient of a scalar differentiable function $\mathcal{L}(\cdot)$ with respect to \mathbf{V} .

A Proof of Thm. 1

For $c \in [k]$, let $\mathcal{C}_c = \{i : y_i = c\}$ be the set of examples belonging to class c , and define $\mathcal{L}_i(\mathbf{H})$ as follows,

$$\begin{aligned} \mathcal{L}_i(\mathbf{H}) &= \sum_{j \in \mathcal{C}_{y_i}, j \neq i} \log \left(\sum_{\ell \in [n], \ell \neq i} \exp(\mathbf{h}_i^\top \mathbf{h}_\ell - \mathbf{h}_i^\top \mathbf{h}_j) \right) \\ &= \sum_{j \in \mathcal{C}_{y_i}, j \neq i} \log \left(\sum_{\ell \in \mathcal{C}_{y_i}, \ell \neq i} \exp(\mathbf{h}_i^\top \mathbf{h}_\ell - \mathbf{h}_i^\top \mathbf{h}_j) + \sum_{\ell \notin \mathcal{C}_{y_i}} \exp(\mathbf{h}_i^\top \mathbf{h}_\ell - \mathbf{h}_i^\top \mathbf{h}_j) \right). \end{aligned} \quad (7)$$

Then, we can rewrite the full-batch SCL in (2) as,

$$\mathcal{L}_{\text{full}}(\mathbf{H}) = \sum_{i \in [n]} \frac{1}{n_{y_i} - 1} \mathcal{L}_i(\mathbf{H}) = \sum_{c \in [k]} \frac{1}{n_c - 1} \sum_{i \in \mathcal{C}_c} \mathcal{L}_i(\mathbf{H}).$$

Now for $c \in [k]$, consider example $i \in \mathcal{C}_c$, and define

$$\mathbf{a}_i := \frac{1}{n_c - 1} \sum_{\ell \in \mathcal{C}_c, \ell \neq i} \mathbf{h}_\ell, \quad \mathbf{b}_i := \frac{1}{n - n_c} \sum_{\ell \notin \mathcal{C}_c} \mathbf{h}_\ell.$$

Note \mathbf{a}_i is the mean-embedding of all examples in class c but i , and \mathbf{b}_i is the mean-embedding of all examples not in class c . Starting from (7), by applying Jensen's inequality to the strictly convex function $f_1(x) := \exp(x - \mathbf{h}_i^\top \mathbf{h}_j)$ we have,

$$\begin{aligned} \mathcal{L}_i(\mathbf{H}) &\geq \sum_{j \in \mathcal{C}_c, j \neq i} \log \left((n_c - 1) \exp(\mathbf{h}_i^\top \mathbf{a}_i - \mathbf{h}_i^\top \mathbf{h}_j) + (n - n_c) \exp(\mathbf{h}_i^\top \mathbf{b}_i - \mathbf{h}_i^\top \mathbf{h}_j) \right) \\ &= \sum_{j \in \mathcal{C}_c, j \neq i} \log \left(((n_c - 1) \exp(\mathbf{h}_i^\top \mathbf{a}_i) + (n - n_c) \exp(\mathbf{h}_i^\top \mathbf{b}_i)) \exp(-\mathbf{h}_i^\top \mathbf{h}_j) \right) \\ &\stackrel{(i)}{=} \sum_{j \in \mathcal{C}_c, j \neq i} \log \left(\alpha_i \exp(-\mathbf{h}_i^\top \mathbf{h}_j) \right) \\ &\stackrel{(ii)}{=} (n_c - 1) \log \left(\alpha_i \exp \left(-\mathbf{h}_i^\top \left(\frac{1}{n_c - 1} \sum_{j \in \mathcal{C}_c, j \neq i} \mathbf{h}_j \right) \right) \right) \\ &= (n_c - 1) \log(\alpha_i \exp(-\mathbf{h}_i^\top \mathbf{a}_i)) \\ &= (n_c - 1) \log \left((n_c - 1) + (n - n_c) \exp \left(\frac{1}{n - n_c} \mathbf{h}_i^\top \sum_{\ell \notin \mathcal{C}_c} \mathbf{h}_\ell - \frac{1}{n_c - 1} \mathbf{h}_i^\top \sum_{\ell \in \mathcal{C}_c, \ell \neq i} \mathbf{h}_\ell \right) \right), \end{aligned} \quad (8)$$

where in (i), we define $\alpha_i := (n_c - 1) \exp(\mathbf{h}_i^\top \mathbf{a}_i) + (n - n_c) \exp(\mathbf{h}_i^\top \mathbf{b}_i)$, and in (ii), we use the fact that the function $f_2(x) := \log(\alpha_i \exp(x))$ is an affine function. Now consider all samples $i \in \mathcal{C}_c$. From (8),

$$\begin{aligned} \frac{1}{n_c - 1} \sum_{i \in \mathcal{C}_c} \mathcal{L}_i(\mathbf{H}) &\geq \sum_{i \in \mathcal{C}_c} \log \left((n_c - 1) + (n - n_c) \exp \left(\frac{1}{n - n_c} \mathbf{h}_i^\top \sum_{\ell \notin \mathcal{C}_c} \mathbf{h}_\ell - \frac{1}{n_c - 1} \mathbf{h}_i^\top \sum_{\ell \in \mathcal{C}_c, \ell \neq i} \mathbf{h}_\ell \right) \right) \\ &\geq n_c \log \left((n_c - 1) + (n - n_c) \exp \left(\frac{1}{n_c(n - n_c)} \sum_{i \in \mathcal{C}_c} \mathbf{h}_i^\top \mathbf{h}_\ell - \frac{1}{n_c(n_c - 1)} \sum_{i \in \mathcal{C}_c} \mathbf{h}_i^\top \mathbf{h}_\ell \right) \right). \end{aligned} \quad (9)$$

In the last line we use Jensen's inequality on $f_3(x) := \log((n_c - 1) + (n - n_c) \exp(x))$ which is strictly convex since $n_c > 1$ and $n - n_c > 0$.

By the ReLU constraints we have $\mathbf{h}_i \geq 0$, $i \in [n]$, which implies $\mathbf{h}_i^\top \mathbf{h}_j \geq 0$, $\forall i, j \in [n]$. Further, by Cauchy-Schwarz inequality $\mathbf{h}_i^\top \mathbf{h}_j \leq \|\mathbf{h}_i\| \|\mathbf{h}_j\| = 1$, with equality achieved if and only if $\mathbf{h}_i = \mathbf{h}_j$. Since f_3 is non-decreasing, we can simplify the bound in (9) as follows,

$$\frac{1}{n_c - 1} \sum_{i \in \mathcal{C}_c} \mathcal{L}_i(\mathbf{H}) \geq n_c \log \left((n_c - 1) + (n - n_c) e^{-1} \right). \quad (10)$$

Summing over all classes $c \in [k]$, we get the final bound on the full-batch SCL:

$$\mathcal{L}_{\text{full}}(\mathbf{H}) = \sum_{c \in [k]} \frac{1}{n_c - 1} \sum_{i \in \mathcal{C}_c} \mathcal{L}_i(\mathbf{H}) \geq \sum_{c \in [k]} n_c \log \left((n_c - 1) + (n - n_c) e^{-1} \right).$$

To achieve the lower-bound, from (10), we require $\mathbf{h}_i = \mathbf{h}_j$ if $y_i = y_j$ and $\mathbf{h}_i^\top \mathbf{h}_j = 0$ otherwise. This requirement also satisfies the equality condition for the Jensen inequalities applied in (8) and (9). Thus, any \mathbf{H} achieving the lower-bound follows an OF geometry (Def. 3), which exists as long as $d \geq k$.

B Proof of Thm. 2

Consider the mini-batch SCL in (4), repeated below for convenience:

$$\mathcal{L}_{\text{batch}}(\mathbf{H}) := \sum_{B \in \mathcal{B}} \sum_{i \in B} \frac{1}{n_{B, y_i} - 1} \sum_{\substack{j \in B \\ j \neq i, y_j = y_i}} \log \left(\sum_{\substack{\ell \in B \\ \ell \neq i}} \exp \left(\mathbf{h}_i^\top \mathbf{h}_\ell - \mathbf{h}_i^\top \mathbf{h}_j \right) \right),$$

Denoting the loss over a batch B by

$$\mathcal{L}_B(\mathbf{H}) := \sum_{i \in B} \frac{1}{n_{B, y_i} - 1} \sum_{\substack{j \in B \\ j \neq i, y_j = y_i}} \log \left(\sum_{\substack{\ell \in B \\ \ell \neq i}} \exp \left(\mathbf{h}_i^\top \mathbf{h}_\ell - \mathbf{h}_i^\top \mathbf{h}_j \right) \right),$$

we have $\mathcal{L}_{\text{batch}}(\mathbf{H}) = \sum_{B \in \mathcal{B}} \mathcal{L}_B(\mathbf{H})$. Now, for a given batch B , we apply Thm. 1 to get the lower bound and conditions for equality:

$$\mathcal{L}_B(\mathbf{H}) \geq \sum_{c \in [k]} n_{B, c} \log \left(n_{B, c} - 1 + (n_B - n_{B, c}) e^{-1} \right).$$

Moreover, equality holds if and only if for every pair of samples $i, j \in B$: $\mathbf{h}_i^\top \mathbf{h}_j = 0$ if $y_i \neq y_j$ and $\mathbf{h}_i = \mathbf{h}_j$ if $y_i = y_j$. With this, the overall loss can be bounded from below by summing the individual lower bounds over different batches:

$$\mathcal{L}_{\text{batch}}(\mathbf{H}) \geq \sum_{B \in \mathcal{B}} \sum_{c \in [k]} n_{B, c} \log \left(n_{B, c} - 1 + (n_B - n_{B, c}) e^{-1} \right),$$

with equality achieved if and only if for every $B \in \mathcal{B}$ and every pair of samples $i, j \in B$, $\mathbf{h}_i^\top \mathbf{h}_j = 0$ if $y_i \neq y_j$ and $\mathbf{h}_i = \mathbf{h}_j$ if $y_i = y_j$. As long as $d \geq k$, the equality conditions of every individual batch can be satisfied simultaneously.

Remark 5 (Comparison to analysis of Graf et al. [Gra+21]). *In Sec. 6.1.1, we have commented on the differences between our proof showing the optimization of mini-batch SCL under **UFM₊** and that of Graf et al. [Gra+21] under the UFM. We further elaborate with an illustrative example below: when optimizing the loss decomposed over a set of mini-batches, it is crucial to consider whether the individual batch minimizers are also overall optimal solutions.*

Consider a simple example: $k = d = 3$, $y_1 = 1, y_2 = 2, y_3 = 3$, $B_1 = \{1, 2\}, B_2 = \{1, 3\}, B_3 = \{2, 3\}$, $\mathcal{B} = \{B_1, B_2, B_3\}$. Let us identify the optimal embeddings for the two scenarios with and without non-negativity constraints on the embedding coordinates.

1. *Without non-negativity (UFM):* the optimal embedding configurations can be shown to be ETF with 2 vectors for every batch, which is simply an antipodal structure. In other words, the batch-wise optimal solutions are $\mathbf{h}_1 = -\mathbf{h}_2, \mathbf{h}_1 = -\mathbf{h}_3$ and $\mathbf{h}_2 = -\mathbf{h}_3$, for the batches B_1, B_2 and B_3 , respectively. However, the batch-wise optimal solutions are infeasible due to their contradictory nature. From [Gra+21], it can be deduced that the overall optimal configuration is instead an ETF with 3 vectors. This example underscores the difficulty in optimizing the loss over every batch separately in case of SCL without non-negativity.
2. *With non-negativity (UFM₊):* our results imply that the optimal embeddings form a 2-OF for every batch, i.e., $\mathbf{h}_1 \perp \mathbf{h}_2, \mathbf{h}_1 \perp \mathbf{h}_3$ and $\mathbf{h}_2 \perp \mathbf{h}_3$, for the batches B_1, B_2 and B_3 , respectively. The three conditions are compatible with each other and the fact that the overall optimal solution is a 3-OF in \mathbb{R}^3 . Therefore, we were able to break down the overall optimization into individual batches.

B.1 Proof of Cor. 2.1

From Thm. 2, the optimal configuration of embeddings in UFM_+ under the mini-batch SCL depends on how batch conditions interact with each other. Specifically, recall that the equality in (5) is achieved if and only if for any batch $B \in \mathcal{B}$, and each pair of samples $(i, j) \in B$, $\mathbf{h}_i = \mathbf{h}_j$ if $y_i = y_j$, and $\mathbf{h}_i^\top \mathbf{h}_j = 0$ otherwise. The OF geometry clearly satisfies all these conditions and achieves the minimal cost of UFM_+ . However, as discussed in Sec. 4.2, these equality conditions may be satisfied by configurations other than OF for an arbitrary batching scheme. So, in Cor. 2.1, we specify the requirements of a batching scheme in order for the global optimal of the mini-batch SCL to be unique (up to global rotations), and match the optimal of the full-batch SCL, which is the OF geometry.

To prove the corollary, we separately address the ‘IF’ and ‘ONLY IF’ parts of the Cor. 2.1.

- **‘IF’ direction.** Assume the batching scheme satisfies both conditions of Cor. 2.1: 1) $\forall c \in [k]$, the induced subgraph G_c is connected, and 2) $\forall c \neq c' \in [k]$, there exists an edge between G_c and $G_{c'}$. We show below that under these two conditions the optimum of UFM_+ under mini-batch SCL follows an OF geometry. In other words, we show that the optimal embeddings align if they belong to the same class (NC) and are orthogonal if they have different labels (mean-embeddings follow k-OF). (See Def. 3.)

NC: Consider a class c . From our assumption, the induced subgraph G_c is connected. Thus, a path exists from any node (representing corresponding example) to any other node in G_c . Consider three nodes⁵ along a path, indexed by i, j, l that belong to class c . Let there be an edge between i, j and j, l each. By Def. 4 of the Batch Interaction Graph, examples i and j are present in a batch, say B_1 , and examples j, l belong to a batch B_2 that is possibly different from B_1 . From Thm. 2, we can infer that at the optimal solution, we have $\mathbf{h}_i = \mathbf{h}_j$, due to equality conditions for batch B_1 . Also, $\mathbf{h}_j = \mathbf{h}_l$, due to equality conditions for batch B_2 . Thus, by transitivity, we have $\mathbf{h}_i = \mathbf{h}_j = \mathbf{h}_l$. Repeating this argument along any path in G_c for every $c \in [k]$, we obtain the NC property: $\mathbf{h}_i = \mathbf{h}_j, \forall i, j : y_i = y_j = c$ for every class $c \in [k]$.

k -OF: From our assumption, for any pair of classes c_1 and c_2 , there exists an edge between G_{c_1} and G_{c_2} connecting at least one pair of nodes $i, j : i \in G_{c_1}, j \in G_{c_2}$. By definition of the Batch Interaction Graph, we know that examples i and j belong in at least one batch. Thus, by Thm. 2, at the optimal solution, we have $\mathbf{h}_i \perp \mathbf{h}_j$ since examples $y_i = c_1 \neq c_2 = y_j$. Now, by NC, $\mathbf{h}_i = \mu_{c_1}, \mathbf{h}_j = \mu_{c_2}$, and thus, $\mu_{c_1} \perp \mu_{c_2}$. This holds for every pair of classes $c_1 \neq c_2 \in [k]$. Therefore, the matrix $\mathbf{M} = [\mu_1, \dots, \mu_k]$ of class-mean embeddings forms a k -OF.

Combining the two statements above, we conclude that at the global optimal solution, the embeddings follow the OF geometry, as desired.

- **‘ONLY IF’ direction.** For the other direction, it suffices to show that if either of the two conditions in Cor. 2.1 does not hold, then there exists an optimizer that does not follow the OF

⁵The same arguments and considerations apply when G_c consists of only two nodes.

geometry. Specifically, we show that when either of the two conditions is violated and $d \geq k + 1$, there exists an embeddings matrix $\tilde{\mathbf{H}}$ attaining the loss lower-bound that does not satisfy one of the two requirements of the OF geometry: 1) $\tilde{\mathbf{H}}$ does not follow NC, or 2) the corresponding mean-embeddings $\tilde{\mathbf{M}}$ do not arrange as a k -OF.

Case 1. Suppose for a $c \in [k]$, the induced subgraph G_c is not connected, and without loss of generality, assume $c = 1$. This means that G_1 has at least two separate components. Denote the nodes in each of the two component by V_1^1 and V_1^2 respectively, and recall for $c \geq 2$, $V_c = \{i : y_i = c\}$. As $d \geq k + 1$, we can choose a set of $k + 1$ vectors $[\tilde{\boldsymbol{\mu}}_1^1, \tilde{\boldsymbol{\mu}}_1^2, \tilde{\boldsymbol{\mu}}_2, \tilde{\boldsymbol{\mu}}_3, \dots, \tilde{\boldsymbol{\mu}}_k]$ such that they form a $(k + 1)$ -OF. Define $\tilde{\mathbf{H}} = [\tilde{\mathbf{h}}_1, \dots, \tilde{\mathbf{h}}_n]$ as follows:

$$\begin{aligned} \forall i \in V_1^1, \quad \tilde{\mathbf{h}}_i &= \tilde{\boldsymbol{\mu}}_1^1 \\ \forall i \in V_1^2, \quad \tilde{\mathbf{h}}_i &= \tilde{\boldsymbol{\mu}}_1^2 \\ \forall i \in V_c, c \in [k], \quad \tilde{\mathbf{h}}_i &= \tilde{\boldsymbol{\mu}}_c. \end{aligned}$$

Then, $\tilde{\mathbf{H}}$ satisfies the equality conditions in Thm. 2 since there is no edge between the nodes in V_1^1 and V_1^2 by the assumption. However, the embeddings in class $y = 1$ do not align, since $\tilde{\boldsymbol{\mu}}_1^1$ is orthogonal to $\tilde{\boldsymbol{\mu}}_1^2$. Thus, $\tilde{\mathbf{H}}$ optimizes UFM_+ while it does not satisfy NC and differs from the OF geometry.

Case 2. Suppose there exists $c_1 \neq c_2 \in [k]$ for which there is no edges between G_{c_1} and G_{c_2} , and without loss of generality, assume $c_1 = 1, c_2 = 2$. Consider an embedding matrix $\tilde{\mathbf{H}}$ that satisfies NC, and the corresponding mean-embedding matrix $\tilde{\mathbf{M}} = [\tilde{\boldsymbol{\mu}}_1, \tilde{\boldsymbol{\mu}}_2, \dots, \tilde{\boldsymbol{\mu}}_k]$ is such that $\forall c \neq c' \in \{2, \dots, k\}$, $\tilde{\boldsymbol{\mu}}_c^\top \tilde{\boldsymbol{\mu}}_{c'} = 0$ and $\tilde{\boldsymbol{\mu}}_1 = \tilde{\boldsymbol{\mu}}_2$. Such an $\tilde{\mathbf{M}}$ exists as $d \geq k$ and all we need is to have $[\tilde{\boldsymbol{\mu}}_2, \dots, \tilde{\boldsymbol{\mu}}_k]$ be a $(k - 1)$ -OF in the non-negative orthant. Since, there is no edge between G_1 and G_2 , there is no $B \in \mathcal{B}$ that includes samples from classes $y = 1$ and $y = 2$ simultaneously. Equivalently, to achieve the lower-bound of Thm. 2, we do not require orthogonality between any pairs of samples $i \in \mathcal{C}_1$ and $j \in \mathcal{C}_2$. Therefore, $\tilde{\mathbf{H}}$ is an optimal solution of the UFM_+ . However, the mean-embeddings do not follow a k -OF. In fact, this optimal geometry, does not distinguish the samples in classes $y = 1$ and $y = 2$.

Therefore, the global minimizer will be uniquely an OF if and only if the batching scheme satisfies both the conditions stated in Cor. 2.1.

C Proofs for Section 6.2

C.1 Proof of Lemma 6.1

Let $\mathbf{V} = [\mathbf{v}_1 \dots \mathbf{v}_k]$ and $\bar{\mathbf{V}} = [\bar{\mathbf{v}}_1 \dots \bar{\mathbf{v}}_k]$. By definition of a k -OF, we know that $\mathbf{V}^\top \mathbf{V} \propto \mathbb{I}$. Without loss of generality suppose the constant of proportionality is 1 so that $\mathbf{V}^\top \mathbf{V} = \mathbb{I}$. Since all \mathbf{v}_i s are orthonormal, this then implies that $\mathbf{V}^\top \mathbf{v}_G = \frac{1}{k} \mathbf{1}_k$ and $\mathbf{v}_G^\top \mathbf{v}_G = \frac{1}{k}$. These put together gives the desired as follows:

$$\bar{\mathbf{V}}^\top \bar{\mathbf{V}} = (\mathbf{V} - \mathbf{v}_G \mathbf{1}_k^\top)^\top (\mathbf{V} - \mathbf{v}_G \mathbf{1}_k^\top) = \mathbf{V}^\top \mathbf{V} - \mathbf{1}_k \mathbf{v}_G^\top \mathbf{V} - \mathbf{V}^\top \mathbf{v}_G \mathbf{1}_k^\top + (\mathbf{v}_G^\top \mathbf{v}_G) \mathbf{1}_k \mathbf{1}_k^\top = \mathbb{I}_k - \frac{1}{k} \mathbf{1}_k \mathbf{1}_k^\top.$$

C.2 Proof of Lemma 6.2

To rule out the optimality of ETF in imbalanced setups, we show ETF does not minimize the loss in a $k = 3$ class example. Specifically, consider a STEP-imbalanced training set with 3 classes of sizes $[Rn_{\min}, n_{\min}, n_{\min}]$ with $n_{\min} \geq 2$ and $R \geq 10$. Suppose \mathbf{H}_{ETF} follows the ETF geometry. Then, from Def. 5 and the feasibility condition, for the mean-embeddings \mathbf{M}_{ETF} we have $\mathbf{M}_{\text{ETF}}^\top \mathbf{M}_{\text{ETF}} = \frac{k}{k-1} (\mathbb{I}_k - \frac{1}{k} \mathbf{1}_k \mathbf{1}_k^\top)$. Thus, the value of the loss function at ETF is

$$\mathcal{L}_{\text{full}}(\mathbf{H}_{\text{ETF}}) = n_{\min} \left(R \log \left(Rn_{\min} - 1 + 2n_{\min} e^{-\frac{3}{2}} \right) + 2 \log \left(n_{\min} - 1 + n_{\min} (R + 1) e^{-\frac{3}{2}} \right) \right).$$

Now, consider $\tilde{\mathbf{H}} = [\tilde{\boldsymbol{\mu}} \otimes \mathbf{1}_{Rn_{\min}}^\top, -\tilde{\boldsymbol{\mu}} \otimes \mathbf{1}_{n_{\min}}^\top, -\tilde{\boldsymbol{\mu}} \otimes \mathbf{1}_{n_{\min}}^\top]$, where $\tilde{\boldsymbol{\mu}}$ is an arbitrary unit-norm vector. Since $\|\tilde{\boldsymbol{\mu}}\| = 1$, it follows that $\tilde{\mathbf{H}}$ is in the feasible set. With this choice of $\tilde{\mathbf{H}}$, we have,

$$\mathcal{L}_{\text{full}}(\tilde{\mathbf{H}}) = n_{\min} \left(R \log(Rn_{\min} - 1 + 2n_{\min}e^{-2}) + 2 \log(2n_{\min} - 1 + Rn_{\min}e^{-2}) \right).$$

It is easy to check that, for imbalance levels higher than $R \geq 10$,

$$\mathcal{L}_{\text{full}}(\tilde{\mathbf{H}}) < \mathcal{L}_{\text{full}}(\mathbf{H}_{\text{ETF}}).$$

In other words, ETF does not always attain the optimal cost in **UFM**.

D Additional experimental results and discussion

D.1 Details on the main experimental setup

In our deep-net experiments, we focus on two common network architectures, ResNet and DenseNet. Specifically, we use ResNet-18 and DenseNet-40 with approximately 11 million and 200 thousand trainable parameters, respectively. For both models, we replace the last layer linear classifier with a normalization layer (normalizing such that $\|\mathbf{h}_i\| = 1$ for $i \in [n]$) of feature dimension $d = 512$. Specifically, following [Gra+21], we directly optimize the normalized features that are then used for inference. (We note this is slightly different compared to [Kho+20], where the authors train the output features of a projection head, then discard this projection head at inference time). We remark that both ResNet and DenseNet architectures include ReLU activations before the final output, which enforces a non-negativity on the learned embeddings. Resnet-18 models with CIFAR10, MNIST and FashionMNIST have been trained for 350 epochs with a constant learning rate of 0.1, no weight decay, batch size of 1024, and SCL temperature parameter $\tau = 0.1$ (consistent with the choice of τ made in [Kho+20; Gra+21]). For all experiments with other models or datasets, we provide experimental details in the following sections. All models, regardless of architecture or dataset, have been trained on a single Tesla V100 GPU machine.

D.2 Additional geometric analysis

In addition to analyzing the convergence of the Gram-matrix of class-mean embeddings \mathbf{G}_M to the OF geometry (as provided in Fig. 2), we also keep track of Neural Collapse (Defn. 1) of individual embeddings and orthogonality of their class-means (Defn. 2) separately. Furthermore, we qualitatively study the Gram matrices \mathbf{G}_M and \mathbf{G}_H and compare them to corresponding matrices for the CE loss under imbalances.

D.2.1 Neural Collapse

In order to quantify the collapse (NC) of embeddings, $\mathbf{h}_i, i \in [n]$, to their class-means, we measure $\beta_{\text{NC}} := \text{tr}(\Sigma_W \Sigma_B^\dagger)/k$ [PHD20]. Here, $\Sigma_B = \sum_{c \in [k]} (\boldsymbol{\mu}_c - \boldsymbol{\mu}_G)(\boldsymbol{\mu}_c - \boldsymbol{\mu}_G)^\top$ is the between class covariance matrix, $\boldsymbol{\mu}_G = \frac{1}{k} \sum_{c \in [k]} \boldsymbol{\mu}_c$ is the global mean, and $\Sigma_W = \sum_{i \in [n]} (\mathbf{h}_i - \boldsymbol{\mu}_{y_i})(\mathbf{h}_i - \boldsymbol{\mu}_{y_i})^\top$ is the within class covariance matrix.

For the experiments shown in Fig. 2 and Fig. 4 in the main body, the corresponding values of β_{NC} can be found in Fig. 10 and Fig. 14(b) respectively.

D.2.2 Angular convergence

Having confirmed convergence of embeddings to their respective class-means via NC ($\mathbf{h}_i \approx \boldsymbol{\mu}_c$ for $i : y_i = c$), we can now compare the feature geometry to the OF geometry by calculating the average $\alpha_{\text{sim}}(c, c') := \boldsymbol{\mu}_c^\top \boldsymbol{\mu}_{c'}/\|\boldsymbol{\mu}_c\| \|\boldsymbol{\mu}_{c'}\|$ between each pair of classes. Fig. 11 plots the average

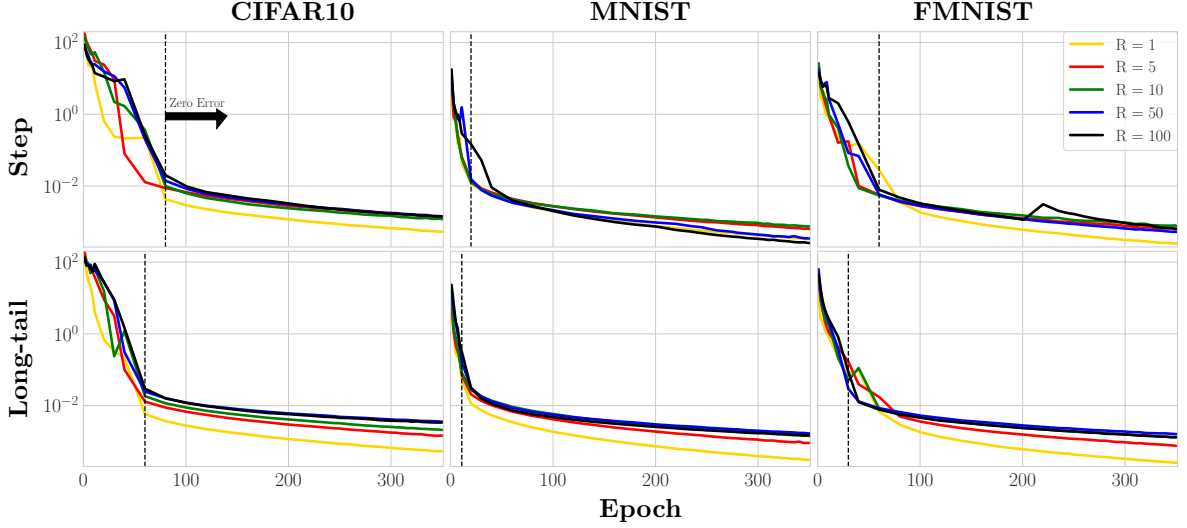


Figure 10: Neural Collapse metric $\beta_{NC} := \text{tr}(\Sigma_W \Sigma_B^\dagger)/k$ for the corresponding ResNet-18 experiments in Fig. 2. Values are usually on the order of 10^{-3} suggesting strong convergence of embeddings to their class means.

cosine similarity $\text{Ave}_{c \neq c'} \alpha_{\text{sim}}(c, c')$ between class means for the same experiment as that of Fig. 2. The graphs indicate strong convergence to orthogonality between feature representations of different classes. Similarly, results for angular convergence corresponding to Fig. 4 are provided in Fig. 14(c), indicating similar convergence to OF for the full-batch experiments.

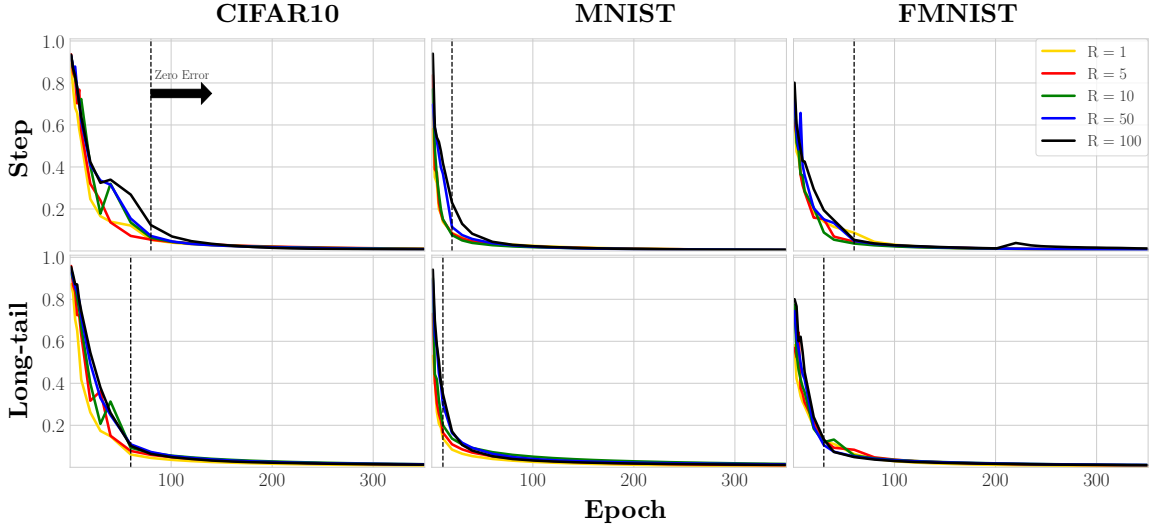


Figure 11: Average cosine similarity between different class means $\alpha_{\text{sim}}(c, c') := \mu_c^\top \mu_{c'}/\|\mu_c\| \|\mu_{c'}\|$ for corresponding results from Fig. 2. Final values are mostly on the order of 10^{-2} , indicating strong orthogonality between class-mean embeddings.

D.2.3 Embedding heatmaps

As a qualitative measure, we have generated heatmaps that visually represent the learned embedding geometries; see Figs. 3, 12, 13. Specifically, we generate heatmaps of the Gram-matrices $\mathbf{G}_M = \mathbf{M}^\top \mathbf{M}$ and $\mathbf{G}_H = \mathbf{H}^\top \mathbf{H}$. In Fig. 3 we train ResNet-18 with the full MNIST dataset. In Fig. 12 we run on a subset of the dataset ($n = 10000$ total examples) with a batch size of 1000. Specifically for Fig. 12, when optimizing with CE loss we modify the network

(ResNet-18) such that it has a normalization layer before the linear classifier head. We consider this additional setting to allow for a comparison where CE features are constrained to the unit sphere akin to our SCL experiments. Lastly, in Fig. 13 we plot the learned features Gram-matrix $\mathbf{G}_\mathbf{H}$ for a ResNet-18 trained on CIFAR10 ($n = 10000$ total examples) with a batch size of 1000.⁶ This heatmap qualitatively shows a more complete picture as we are plotting $\mathbf{G}_\mathbf{H} = \mathbf{H}^\top \mathbf{H}$ rather than $\mathbf{G}_\mathbf{M}$, thus simultaneously illustrating both Neural Collapse and convergence to the k-OF structure.

D.2.4 Experiments with MLPs

In Fig. 16 we run experiments with a simple 6 layer multilayer perceptron (MLP) to further explore the impact of model complexity on geometric convergence. The MLP includes batch normalization and ReLU activation between each layer. Each layer has 512 hidden units. We train the model with a batch size of 1000 with random reshuffling at each epoch. Furthermore, we train under R -STEP imbalanced MNIST. No batch duplication was used. All other aspects of the implementation are as described in Sec. D.1. As shown in Fig. 16 all metrics $\Delta\mathbf{G}_\mathbf{M}$, β_{NC} , and $\text{Ave}_{c \neq c'} \alpha_{\text{sim}(c, c')}$ indicate strong convergence to the OF geometry, irrespective of imbalance ratio R .

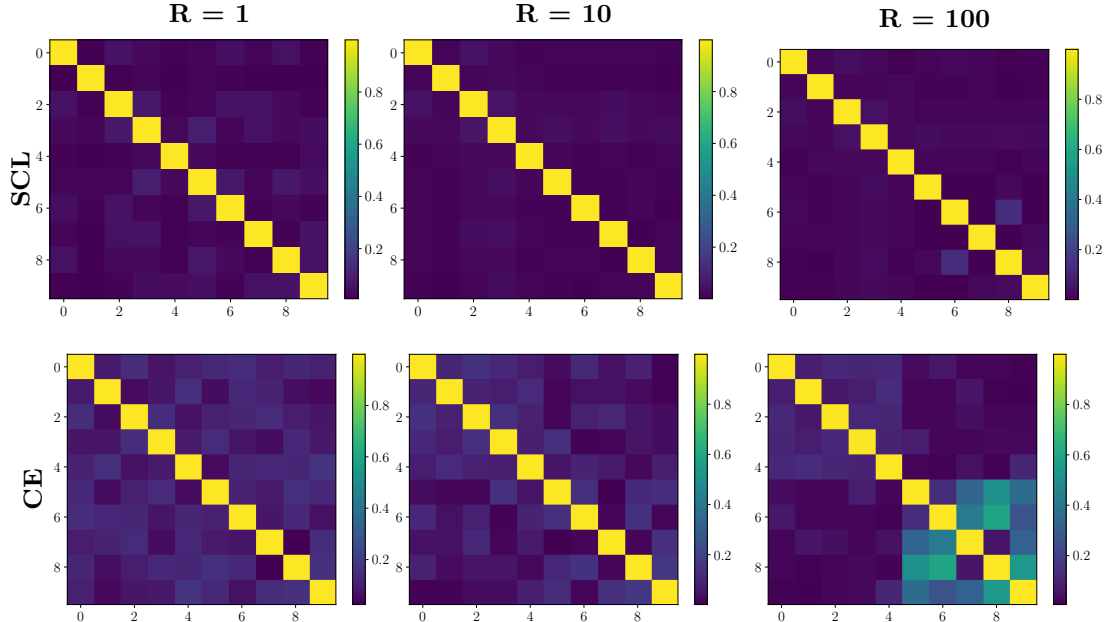


Figure 12: $\mathbf{G}_\mathbf{M}$ Gram-matrices of mean-embeddings for various R -STEP imbalances at last epoch (350) of training with ResNet-18 on MNIST with $n = 10000$. To allow for fair comparison, the CE features are normalized before the classifier head akin to the SCL experiments.

D.3 Optimization dynamics

D.3.1 Loss convergence

In order to compute the lower bounds shown in Fig. 4, we use Thm. 1, substituting e^{-1} with $e^{-1/\tau}$ using $\tau = 0.1$ as employed in our experiments; this substitution is allowed thanks to Remark 2. Furthermore, we compute the lower bounds and $\mathcal{L}(\mathbf{H})$ on a per sample basis, thus we divide by $n = 1000$ which corresponds to the number of datapoints in our single batch. Lastly, as a

⁶In both Fig. 13 and Fig. 12 no batch duplication is used as described in Sec. 3.

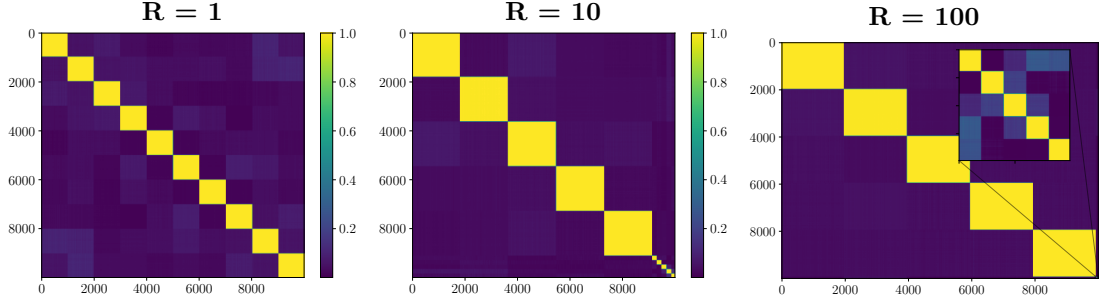


Figure 13: \mathbf{G}_H Gram-matrices of feature embeddings for various imbalances at last epoch (350) of training SCL with CIFAR10 and ResNet.

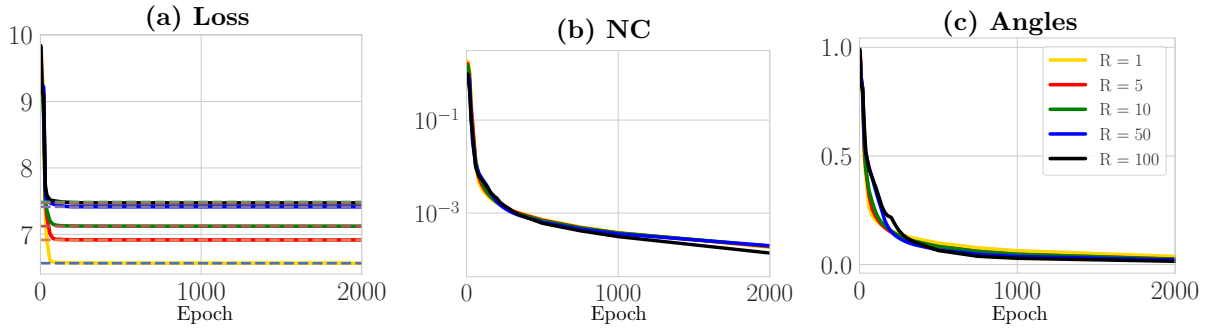


Figure 14: Full-batch SCL: ResNet-18 trained on a R -STEP imbalanced subset of MNIST of size $n = 1000$. (a) Loss converges to the lower bound (dashed lines) computed in Thm. 1. (b) Within-class feature variation becomes negligible (NC). (c) The average pairwise cosine similarity of class-means approaches zero. Each epoch is equivalent to one iteration of gradient descent.

method of maintaining numerical stability (as implemented in [Kho+20]) we apply a global scaling of the loss by a factor τ/τ_b , where $\tau_b = 0.07$ is the base temperature [Kho+20]. The complete experiment, conducted over 2000 epochs (with axes limited to 500 epochs for clarity in Figure 4), is available in Figure 14.

D.3.2 Effect of τ

As described in Sec. 3 and Sec. 4.1 the optimality of the OF geometry for the UFM_+ is invariant to the choice of the temperature parameter τ . However, we have found that the speed of convergence to the OF geometry is dependent on the choice of τ . Shown in Fig. 15 is a full batch SCL experiment on $n = 1000$ samples of MNIST trained on ResNet-18 with $\tau = 0.1, 1, 10$. It is clear from Fig. 15 that: (a) the within-class feature variation converges significantly faster for smaller τ ; (b) the angles converge to k-OF faster and smoother for smaller τ as well (see Fig. 15 (b)). In all cases, values of β_{NC} and $\alpha_{\text{sim}}(c, c')$ continue to decrease, and we anticipate further convergence if the networks are trained for longer. These results qualitatively agree with the findings of [Kho+20] which suggest that smaller τ improves training speed.

D.4 Complementary results and discussions on batch-binding

In this section, we describe examples where batching methods and batch-binding help improve the convergence speed of embeddings geometries to OF.

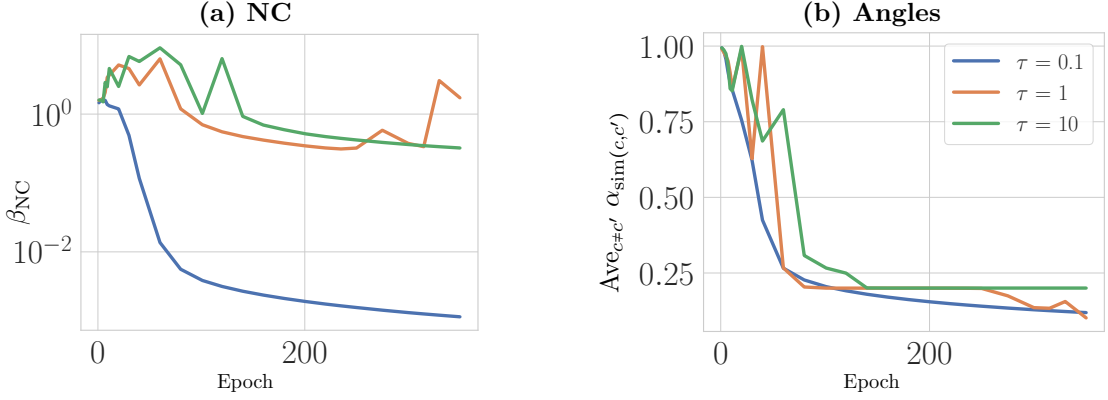


Figure 15: Full-batch SCL: ResNet-18 trained on a subset of MNIST of size $n = 1000$ with different temperature parameters τ . (a) Within-class feature variation (NC). (b) Average pairwise cosine similarity of class-means. Each epoch is equivalent to one iteration of gradient descent.

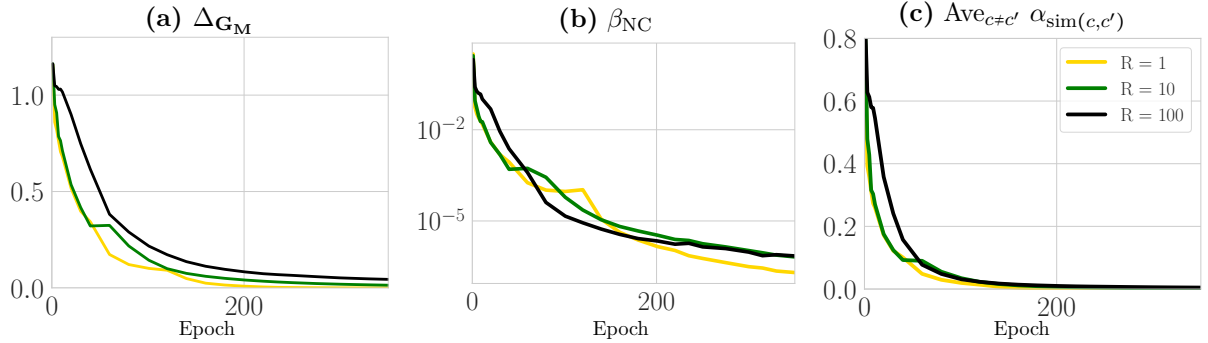


Figure 16: Geometry convergence metrics (a) Δ_{GM} , (b) β_{NC} , and (c) $\text{Ave}_{c \neq c'} \alpha_{\text{sim}(c,c')}$ for a 6 layer multilayer perceptron (MLP) model with ReLU activations trained with SCL and MNIST under R -STEP imbalance.

D.4.1 How batch-binding ensures a unique OF geometry

Fig. 17 provides a simple illustration demonstrating how adding binding examples can satisfy the requirements of Cor. 2.1. While there are alternative approaches to satisfy the graph conditions stated in Cor. 2.1 for ensuring a unique OF geometry, the method of adding the same k examples to each batch is a straightforward technique that is often computationally efficient, considering that batch sizes typically exceed the number of classes k .

Table 1: NCC test accuracy for Batch-Binding

Ratio (R)	Step		Long-tail	
	Reshuffling	Reshuffling + Batch-Binding	Reshuffling	Reshuffling + Batch-Binding
10	$83.31 \pm 0.65\%$	$83.27 \pm 0.27\%$	$85.04 \pm 0.28\%$	$85.03 \pm 0.57\%$
100	$64.07 \pm 1.79\%$	$64.18 \pm 1.25\%$	$67.75 \pm 1.21\%$	$68.08 \pm 0.72\%$

D.4.2 Impact of batch-binding on generalization

To study the effect of binding examples on generalization, we consider the *Nearest Class Center* (NCC) classifier. For this, each test example is assigned the label of the class center μ_c learned

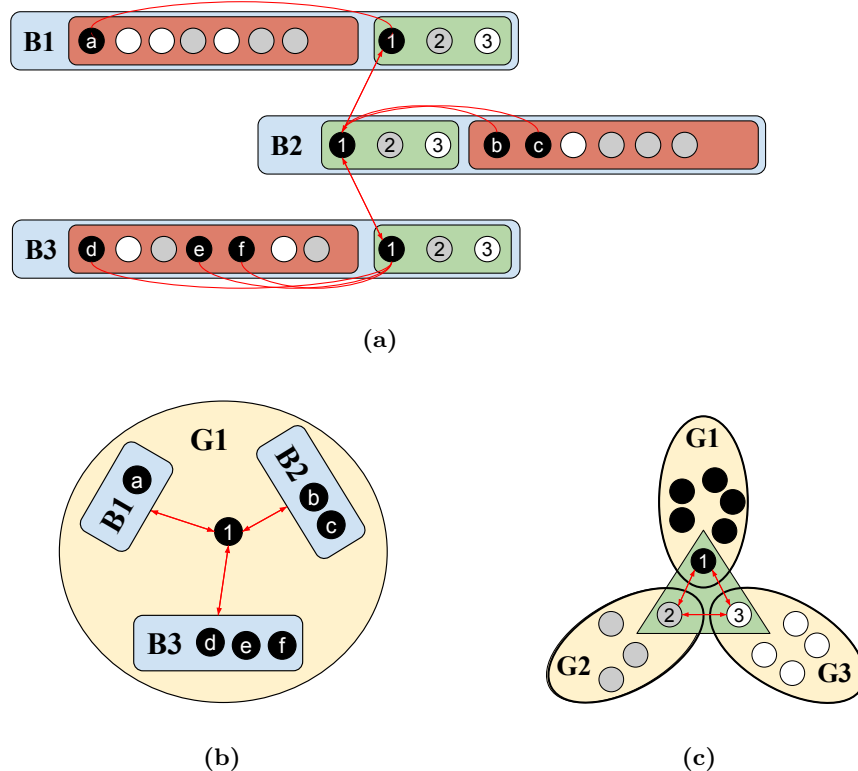


Figure 17: A simple illustration to explain how adding binding examples to each batch satisfies the requirements of Cor. 2.1, thus leads to unique OF geometry. (a) Gives a 3 class (black, grey and white) classification example with 3 batches. In addition to the data for each batch (included in red), the binding examples 1, 2, 3 are added to each batch. (b) Gives the Batch Interaction Graph for the induced subgraph G_1 of the class (black) of example 1 and illustrates how all batches are connected through examples 1, satisfying the first condition of Cor. 2.1. (c) Elaborates on how all three class graphs G_1, G_2, G_3 are connected through the interactions of data points 1, 2, 3, satisfying the second condition of Cor. 2.1.

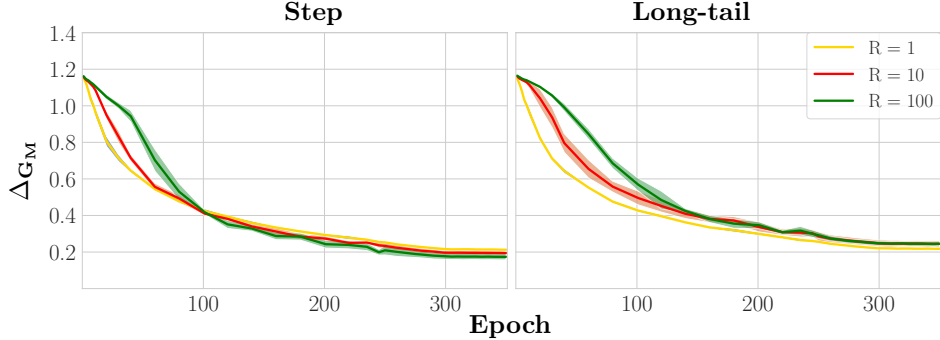


Figure 18: Convergence of \mathbf{G}_M to the OF geometry for a ResNet-18 model trained on CIFAR10 under STEP imbalance, with data augmentation. Results represent the average run results over 5 versions of the experiments with randomly chosen binding examples from each class.

during training that is closest to it (in Euclidean distance). We consider a simple setup of training a ResNet-18 model on CIFAR10 under imbalances $R = 10, 100$ both with and without the binding examples. Models are trained with a batch size of 128 for 350 epochs. We ran the experiments with a smaller batch size to increase the number of back-propagation steps as adding data augmentations slows down convergence to OF geometry. We start with a learning rate of 0.1, which is reduced by a factor of 10 on epochs 250 and 300. Weight decay is set to 5×10^{-4} . In addition, we apply data augmentation as it is common practice when considering generalization and test accuracy. In particular, rather than simply adding horizontally flipped images (as described in Sec. 3) we allow for generic augmentations that include simple horizontal or vertical flips and random cropping with a probability of 0.5. The NCC test accuracy was measured across 5 versions of the experiment with the k binding examples sampled randomly every time and 5 versions without any batch-binding. The results for NCC balanced test accuracies are provided in Table 1. While making definitive conclusions regarding the impact of the embeddings geometries and binding examples on generalization requires further investigation, this preliminary investigation suggests that batch-binding does *not* negatively impact NCC test accuracy.

Finally, Fig. 18 shows convergence of embeddings geometry to OF for the same experiments. As expected, the convergence is slightly slower in this case due to the inclusion of data augmentation (random crops and flips).

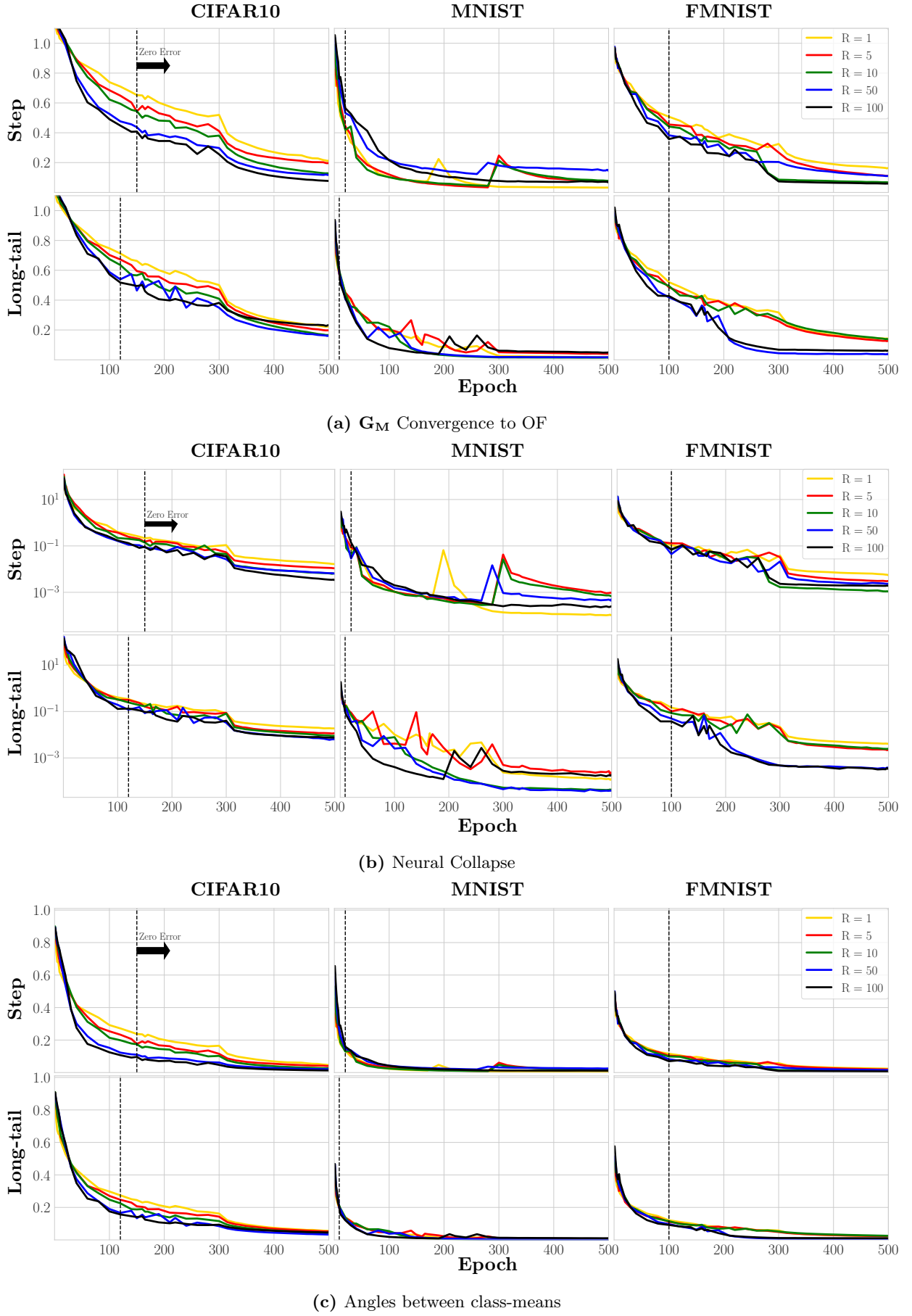


Figure 19: Geometric convergence of embeddings (as based on Def. 1, Def. 2, and Def. 3) of DenseNet-40 trained with batch-binding. We measure: **(a)** $\Delta_{\mathbf{G}_M}$, **(b)** β_{NC} , and **(c)** $\text{Ave}_{c \neq c'} \alpha_{\text{sim}}(c, c')$ as defined in text.